OXFORD

Glycan Synthesis

Tannerella forsythia strains display different cell-surface nonulosonic acids: biosynthetic pathway characterization and first insight into biological implications

Valentin Friedrich[2,†], Bettina Janesch[2,6,†], Markus Windwarder[3],
Daniel Maresch[3], Matthias L Braun[2], Zoë A Megson[2,7],
Evgeny Vinogradov[4], Marie-France Goneau[4], Ashu Sharma[5],
Friedrich Altmann[3], Paul Messner[2], Ian C Schoenhofen[4,1],
and Christina Schäffer[2,1]

[2]Department of NanoBiotechnology, *NanoGlycobiology* Unit, Universität für Bodenkultur Wien, Muthgasse 11, A-1190 Vienna, Austria, [3]Department of Chemistry, Universität für Bodenkultur Wien, Muthgasse 18, A-1190 Vienna, Austria, [4]National Research Council, Human Health Therapeutics Portfolio, 100 Sussex Drive, Ottawa, ON, Canada K1A 0R6, and [5]Department of Oral Biology, School of Dental Medicine, University at Buffalo, 311 Foster Hall, 3435 Main St. Buffalo, New York 14214, USA

[1]To whom correspondence should be addressed: Tel: +43-1-47654-80203; Fax: +43-1-478-9112; e-mail: christina.schaeffer@boku.ac.at (C.S.); Tel: +1-613-991-2141, Fax: +1-613-990-0855, e-mail: Ian.Schoenhofen@nrc-cnrc.gc.ca (I.C.S.)

[6]Present address: Department of Chemistry and Biology, Ryerson University, 350 Victoria Street, Toronto, Ontario, Canada M5B 2K3

[7]Present address: Sandoz GmbH, Biochemiestraße 15, A-6336 Langkampfen, Austria

[†]These authors contributed equally to this work.

Abstract

Tannerella forsythia is an anaerobic, Gram-negative periodontal pathogen. A unique *O*-linked oligosaccharide decorates the bacterium's cell surface proteins and was shown to modulate the host immune response. In our study, we investigated the biosynthesis of the nonulosonic acid (NulO) present at the terminal position of this glycan. A bioinformatic analysis of *T. forsythia* genomes revealed a gene locus for the synthesis of pseudaminic acid (Pse) in the type strain ATCC 43037 while strains FDC 92A2 and UB4 possess a locus for the synthesis of legionaminic acid (Leg) instead. In contrast to the NulO in ATCC 43037, which has been previously identified as a Pse derivative (5-*N*-acetimidoyl-7-*N*-glyceroyl-3,5,7,9-tetradeoxy-L-*glycero*-L-*manno*-NulO), glycan analysis of strain UB4 performed in this study indicated a 350-Da, possibly *N*-glycolyl Leg (3,5,7,9-tetradeoxy-D-*glycero*-D-*galacto*-NulO) derivative with unknown C5,7 *N*-acyl moieties. We have expressed, purified and characterized enzymes of both NulO pathways to confirm these genes' functions. Using capillary electrophoresis (CE), CE–mass spectrometry and NMR spectroscopy, our studies revealed that Pse biosynthesis in ATCC 43037 essentially follows the UDP-sugar route described in *Helicobacter pylori*, while the pathway in strain FDC 92A2 corresponds to Leg biosynthesis in *Campylobacter jejuni* involving GDP-sugar intermediates. To demonstrate that the NulO biosynthesis enzymes are functional in vivo, we created knockout mutants resulting in glycans

lacking the respective NulO. Compared to the wild-type strains, the mutants exhibited significantly reduced biofilm formation on mucin-coated surfaces, suggestive of their involvement in host-pathogen interactions or host survival. This study contributes to understanding possible biological roles of bacterial NulOs.

Introduction

Nonulosonic acids (NulOs) are a class of 9-carbon sugars that are α-keto acids. The most abundant naturally occurring NulOs are the sialic acids (Sia or neuraminic acids, Neu) and their derivatives (Varki 1992; Traving and Schauer 1998). It is established knowledge that Sias play crucial roles in the life-cycles of various organisms from eukaryotes to prokaryotes (Varki et al. 2009). While Sias are commonly present as terminal residues of many eukaryotic glycoconjugates and have also been identified in several prokaryotic polysaccharides, a number of NulOs appear to be unique to bacterial species (Knirel et al. 2003; Morrison and Imperiali 2014; Zunk and Kiefel 2014; Kenyon et al. 2015; Schäffer and Messner 2016). Due to their structural and biosynthetic similarities to Sia, these NulOs are also often referred to as Sia-like sugars (Figure 1A), the most studied of which are pseudaminic acids (such as 5,7-diacetamido-3,5,7,9-tetradeoxy-L-*glycero*-L-*manno*-NulO, Pse5,7Ac$_2$) and legionaminic acids (such as 5,7-diacetamido-3,5,7,9-tetradeoxy-D-*glycero*-D-*galacto*-NulO, Leg5,7Ac$_2$). For both pseudaminic acid (Pse) and legionaminic acid (Leg), several naturally occurring derivatives have been identified. These most commonly include substitutions of the N-acyl groups at the C-5 and C-7 positions, e.g., with N-acetyl or acetamido (Ac), N-acetimidoyl or acetamidino (Am), N-formyl (Fo) and N-hydroxybutyryl (Hb) groups (Zunk and Kiefel 2014).

Pse was first identified in the O-polysaccharide chain of the lipopolysaccharide (LPS) from *Pseudomonas aeruginosa* and *Shigella boydii* (Knirel et al. 1984). Since then, Pse and derivatives have been frequently found as constituents of cell surface glycoconjugates such as pili (Horzempa et al. 2006), flagella (Thibault et al. 2001; Schirm et al. 2003), LPS (Knirel et al. 2003) and capsular polysaccharides (Kiss et al. 2001; Kenyon et al. 2014). In *Campylobacter jejuni*, *Helicobacter pylori* and *Aeromonas* spp., heavy glycosylation of the flagellin protein with Pse has been shown to be an essential requirement for flagellar assembly and, thus, motility and virulence of these pathogens (Guerry et al. 2006; Wilhelms et al. 2012; Lowry et al. 2014).

Leg—a C5,7,8 isomer of Pse (Figure 1A)—was first characterized in a repeating homopolymer of the LPS O-antigen from *Legionella pneumophila*, the causative agent of Legionnaires' disease (Knirel et al. 1994). Since then, Leg and its derivatives have also been found in the LPS of various other Gram-negative bacteria such as *Vibrio salmonicida* (Edebrink et al. 1996), *Pseudomonas fluorescens* (Knirel et al. 1996), *Acinetobacter baumannii* (Haseley and Wilkinson 1997), *Cronobacter turicensis* (MacLean et al. 2011), *Salmonella arizonae* (Vinogradov et al. 1992) and certain serotypes of *Escherichia coli* (Li et al. 2010). Leg has also been found as a major component in the O-linked glycosylation of flagellins in *Campylobacter* spp. (McNally et al. 2007; Schoenhofen et al. 2009) and *Clostridium botulinum* (Twine et al. 2008), the latter marking the first occurrence of a Sia-like sugar in the glycosylation of a Gram-positive flagellar protein. While modification of *C. jejuni* flagellins with a NulO is required for flagellin assembly and motility, the specific NulO present may impart particular

biological consequences, such as seen in a strain lacking the ability to display a 5-N-acetimidoyl Leg derivative (Leg5Am7Ac). This strain exhibited decreased cell hydrophobicity, reduced biofilm formation, and reduced ability to colonize the chicken intestine (Howard et al. 2009).

Apart from some evidence for involvement in bacterial fitness and pathogenicity of distinct organisms, the function of Sia-like sugars as part of cell surface components is still largely unknown. It was suggested that bacterial NulOs could play a role as molecular mimic of eukaryotic Sia, thereby contributing to the pathogen's ability to evade or modulate the host's immune responses (Carlin et al. 2009). A recent study proposes that Pse derivatives on the flagella of *C. jejuni* interact with host Siglec-10 to increase IL-10 expression, thus promoting an anti-inflammatory response and host persistence (Stephenson et al. 2014). In contrast to the scarcity of evidence for their function, an increasing number of studies suggests that Leg and Pse derivatives are widespread among prokaryotes, where more than 20% of 1000 microbial genomes examined were found to encode a predicted NulO biosynthesis pathway (Lewis et al. 2009).

In our group, the ATCC 43037 type strain of the periodontal pathogen *Tannerella forsythia* was found to display a Pse derivative as the terminal residue of its abundant cell surface (S-) layer O-glycans (Figure 1B) (Posch et al. 2011). *T. forsythia* is a Gram-negative anaerobe that inhabits subgingival plaque biofilms in the human oral cavity (Tanner et al. 1986). Together with *Porphyromonas gingivalis* and *Treponema denticola* it forms the so-called "red complex" consortium of oral pathogens, which is strongly associated with periodontal diseases in humans (Holt and Ebersole 2005). Periodontitis is a multifactorial inflammatory disease which progresses as a result of the direct effects of bacterial virulence factors on host tissues, as well as self-damaging host responses to the colonizing bacteria (Socransky et al. 1998; Hajishengallis and Lamont 2012). Apart from being the most common cause of tooth loss worldwide and affecting millions of people (Darveau 2010), periodontitis is increasingly linked to systemic diseases such as cardiovascular disease (Leishman et al. 2010). Among the identified virulence factors of *T. forsythia* is its S-layer (Lee et al. 2006; Sakakibara et al. 2007; Sharma 2010). S-Layers are found as the outermost cell envelope component of many bacteria and archaea (Sára and Sleytr 2000); the constituting (glyco)proteins are predominantly water-insoluble and endowed with the intrinsic capability of self-assembling into 2D crystalline arrays (Schäffer and Messner 2004). Apart from their role as virulence factors, S-layers can have many functions in bacterial growth and survival, including the maintenance of cell integrity, enzyme display and, in pathogens and commensals, interaction with the host and its immune system (Fagan and Fairweather 2014).

Compared to other S-layer-carrying bacteria, *T. forsythia*'s status is unique in two ways: it is the only Gram-negative bacterium that is known to possess a glycosylated S-layer and its S-layer is
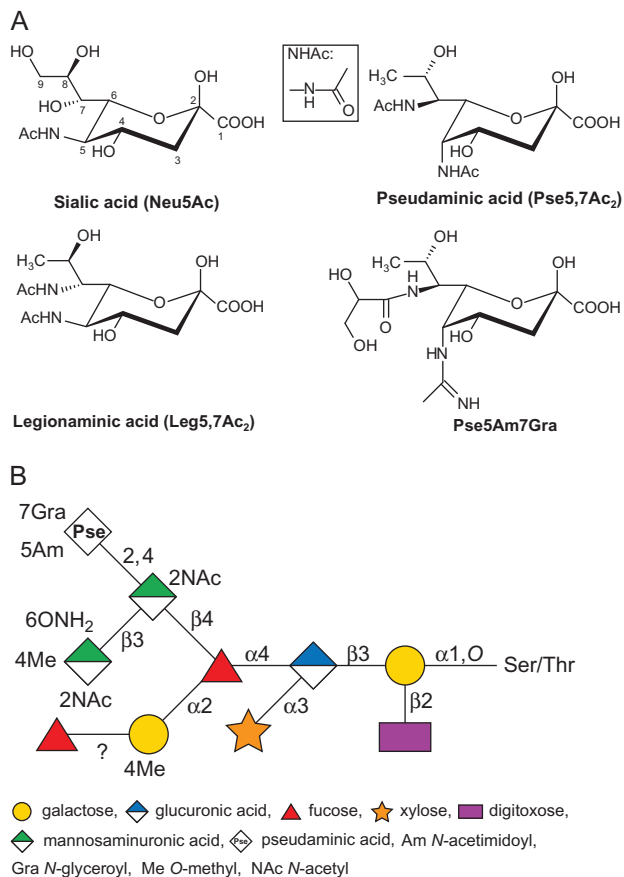
Fig. 1. (**A**) Structures of Sia and Sia-like sugars (NulOs). Sialic acid (Neu5Ac), legionaminic acid (Leg5,7Ac$_2$) and pseudaminic acids (Pse5,7Ac$_2$ and Pse5Am7Gra) are shown. To note, Pse5Am7Gra is found as the terminal sugar of the S-layer glycan in *T. forsythia* ATCC 43037. For reference, the nine carbon atoms of Sia are numbered, and the structure of the NHAc group is shown in the boxed inset. (**B**) Schematic drawing of the structure of the S-layer *O*-glycan in *T. forsythia* ATCC 43037 (amended from Posch et al. (2011)). This figure is available in black and white in print and in color at *Glycobiology* online.

comprised of two S-layer proteins (named TfsA and TfsB) instead of just one (Sekot et al. 2012). After the *T. forsythia* S-layer had been found to delay the host immune response, at least at the early stage of infection, (Sekot et al. 2011), a detailed investigation of the bacterium's cell surface architecture (Sekot et al. 2013) and glycosylation ensued (Posch et al. 2011). As previously mentioned, the S-layer of the ATCC 43037 type strain was shown to be modified with an *O*-linked oligosaccharide containing several rare sugar residues (Figure 1B), including a Pse derivative with an *N*-acetimidoyl (Am) group at C-5 and an *N*-glyceroyl (Gra) group at C-7 (Pse5Am7Gra; Figure 1A; (Sekot et al. 2011)). The original publication by our group correctly identified the C-7 modification by NMR spectroscopy but erroneously described it as an "*N*-glycolyl (Gc)" group. The correct term for this modification is "*N*-glyceroyl", with "Gra" as the proposed abbreviation, although the designation "*N*-2,3-dihydroxypropionyl", "glycerate group" or "glyceric acid" is also in use for this substitution (Thibault et al. 2001; Vinogradov et al. 2009). Interestingly, the S-layer glycan is also present on several other proteins, residing mainly in the outer membrane, indicative of the presence of a general protein *O*-glycosylation system in *T. forsythia* that gives rise to a rich glycoproteome. Considering the prominent location of the modified Pse5Am7Gra as a terminal non-reducing

residue of the outermost cell surface decoration of *T. forsythia*, it is likely to participate in bacterium-host interactions and impact the bacterium's life-style. First indications of this role can be inferred from immunologic studies showing that the *O*-glycan's terminal trisaccharide branch containing the Pse5Am7Gra residue dampens T-helper 17 differentiation, mitigates neutrophil infiltration to the gingival tissue, and increases periodontal bone loss in mice (Settem et al. 2013).

In light of these findings, we launched an investigation into the NulO biosynthetic pathway of *T. forsythia*, which relied primarily on knowledge of the Pse and Leg biosynthesis pathways in *H. pylori* (Schoenhofen et al. 2006b) and *C. jejuni* (Schoenhofen et al. 2009), respectively. In both cases, CMP-NulO, representing the activated form of NulO required for its incorporation into glycoconjugates, is formed by the subsequent action of six enzymes starting from nucleotide-activated *N*-acetylglucosamine. While the pathway to Pse utilizes UDP-GlcNAc as a precursor, Leg biosynthesis in *C. jejuni* was shown to involve GDP-GlcNAc. Apart from using different sugar nucleotides, the biosynthetic routes for Pse and Leg differ in the reactions performed at the C-2, C-4 and C-5 positions of the hexose intermediates, which results in stereochemical differences at C-5, C-7 and C-8 positions in the final NulO (Figure 2). In the first enzymatic step of the Leg pathway, the dehydratase LegB catalyzes a C-4,6 dehydration, while the corresponding enzyme of the Pse pathway, PseB, additionally performs a 5-epimerization reaction. The subsequent amino transfer at C-4 introduces another stereochemical distinction as an axial (PseC) vs. equatorial (LegC) addition of the amino group is performed. After N-4 acetylation (PseH/LegH), NDP removal catalyzed by LegG results in C-2 epimerization, whereas the corresponding enzyme of the Pse biosynthesis pathway, PseG, only possesses NDP-sugar hydrolase activity. In both NulO routes, the formation of the 9-carbon-backbone sugar is catalyzed by homologous enzymes (PseI/LegI) *via* the condensation of a 6-carbon hexose intermediate with the 3-carbon molecule pyruvate. The final enzymatic step, accomplished by PseF/LegF, CMP-activates the free NulO residue using cytidine triphosphate.

A previous bioinformatic analysis of the *T. forsythia* ATCC 43037 type strain genome revealed the presence of a protein *O*-glycosylation gene cluster encoding genes involved in sugar biosynthesis, glycan assembly and transport (Posch et al. 2011). The identification of a dedicated NulO biosynthesis gene locus of *T. forsythia*—as can be found in *H. pylori* (Schoenhofen et al. 2006b) and *C. jejuni* (Schoenhofen et al. 2009)—was complicated by the fact that the publicly available genome thought to match the ATTC 43037 type strain, was in fact derived from *T. forsythia* strain FDC 92A2 (or ATCC BAA-2717). After the discovery of this strain misattribution, we obtained the correct genome sequence of the type strain (Friedrich et al. 2015). In this current work, a bioinformatic analysis of both genomes as well as that of a new *T. forsythia* isolate, strain UB4, predicted a gene locus for Pse biosynthesis in the type strain ATCC 43037, while the genes in strain FDC 92A2 and UB4 pointed towards a Leg biosynthetic route. To confirm the function of the predicted NulO enzymes encoded by these loci and hence the resulting NulO type present in each organism, we have biochemically characterized five enzymes for Pse synthesis (homologs of PseB, PseC, PseH, PseG and PseI) in the type strain and the three stereochemically defining enzymes (homologs of LegB, LegC and LegG) of strains FDC 92A2/UB4. By deleting one of the NulO biosynthetic genes in either pathway, we created knockout mutants displaying *O*-glycans deficient in their respective terminal NulO, thus demonstrating that the NulO biosynthesis
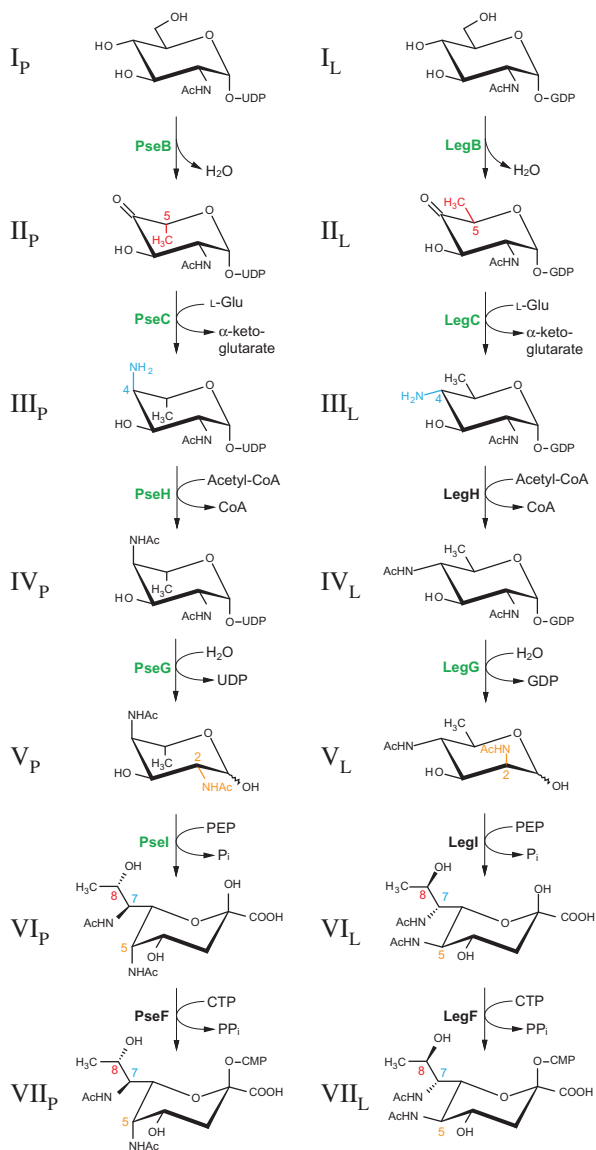
Fig. 2. Experimentally confirmed enzymatic steps (in green) in *T. forsythia* strains ATCC 43037 (left) and FDC 92A2/UB4 (right) corresponding to the CMP-Pse and CMP-Leg biosynthetic pathways as elucidated in *H. pylori* and *C. jejuni*, respectively (Schoenhofen et al. 2006b, Schoenhofen et al. 2009). In *T. forsythia*, pathways will deviate at some point to produce the unique NulO derivatives found in our strains, such as Pse5Am7Gra. These deviations would be anticipated to occur either within the NulO biosynthetic pathway or post CMP-NulO biosynthesis. Red, blue and orange highlight enzymatic steps that introduce the stereochemical differences between the two pathways and also indicate the positions altered for both hexose intermediates and final NulO. The assignment of roman numerals to each compound is consistent with label designations found throughout the text. Subscripts "P" and "L" indicate intermediates from the CMP-Pse and CMP-Leg biosynthesis pathway, respectively. For simplicity, all sugars except for the NulOs are shown in $^4C_1$ form. This figure is available in black and white in print and in color at *Glycobiology* online.

genes are indeed transcribed and the enzymes are functional in vivo. As a first indication of a biological function, we assessed biofilm formation in wild-type and NulO-deficient mutants of *T. forsythia*. Our findings provide a basis for determining the roles of Pse and Leg in the pathogenicity of *T. forsythia* and may contribute to understanding the influence of NulOs on the physiology and life-style of this bacterium.

Results

Bioinformatic analysis of NulO biosynthetic gene loci in three *T. forsythia* strains

The presence of terminal Pse5Am7Gra on the S-layer glycan of *T. forsythia* ATCC 43037 type strain prompted an investigation of the genes involved in the biosynthesis of this NulO. For a comparative genomic analysis, we selected enzymes of the flagellin *O*-linked glycosylation systems of *C. jejuni* 11168 and *H. pylori*. These organisms possess well-characterized biosynthetic pathways to Pse, as well as Leg and Neu in the former (Schoenhofen et al. 2006b; Schoenhofen et al. 2009).

An investigation of the *T. forsythia* ATCC 43037 genome (JUET00000000) recently obtained by our laboratory (Friedrich et al. 2015) revealed the presence of candidate genes for all six dedicated Pse biosynthesis genes (Supplementary Figure 1). They cluster in a locus downstream of a proposed *wzx* flippase gene (Tanf_01180) and upstream of the predicted *T. forsythia* protein *O*-glycosylation gene locus (Posch et al. 2011). All NulO genes showed much higher similarity to the *C. jejuni*/*H. pylori* Pse biosynthetic genes than to the Leg counterparts of *C. jejuni* (Table I). The presence of a homolog to PseB (Tanf_01185), in particular, was a strong indication towards Pse, as this enzyme is unique among other dehydratases in its ability to additionally perform a C-5 epimerization (McNally et al. 2008).

A homology search of *C. jejuni* NulO biosynthesis amino acid sequences against the genomes of strains FDC 92A2 (Genbank CP003191) and UB4 (Stafford et al. in preparation) revealed major differences with respect to the genome of strain ATCC 43037. The putative flippase gene (Tanf_01180/BFO_1075) is identical in FDC 92A2, UB4 and the type strain along almost its entire length, however, alignment breaks down over the last 30 base pairs (Supplementary Figure 1). Downstream of this ORF is a locus of NulO biosynthetic genes that is identical in FDC 92A2 and UB4 but exhibits no significant similarity to the putative Pse biosynthesis locus found in strain ATCC 43037, regarding both the arrangement and types of genes. The first gene that shows homology between the strains again is an ORF at the 5′-end of the locus which encodes a hypothetical protein (BFO_1060), the C-terminal half of which is identical to the corresponding gene in the type strain (Tanf_01245). A closer inspection of the NulO biosynthesis genes found in this genomic locus suggested that strains FDC 92A2 and UB4 possess the biosynthetic route towards Leg (Table I). Firstly, for the dehydratase (LegB/PseB), aminotransferase (LegC/PseC), NulO synthase (LegI/PseI) and CMP-activating synthetase (LegF/PseF), strains FDC 92A2/UB4 genes display higher similarity to the Leg biosynthetic enzymes of *C. jejuni* than to those of the Pse pathway. Secondly, no PseG or UDP-sugar hydrolase consensus sequence could be identified, while there is a good candidate for the hydrolyzing 2-epimerase LegG. This strongly supported Leg synthesis as 2-epimerization does not occur in the Pse pathway. Lastly, the presence of a homolog to the nucleotidyl transferase PtmE points towards a biosynthetic pathway utilizing a GDP-linked intermediate. With respect to activator NTP donors, PtmE has been shown to be absolutely specific for GTP in reactions involving the abundant hexosamine metabolite GlcN-1-P, converting it to GDP-GlcN where GDP-GlcNAc is the LegB substrate in *C. jejuni* (Schoenhofen et al. 2009). The Pse pathway, on the other hand, would likely require UDP-GlcNAc as a precursor. Even though there are no good matches for the *N*-acetyltransferase LegH, the gene BFO_1067 encodes an amino acid sequence that is similar to PglD, an *N*-acetyltransferase involved in UDP-2,4-diacetamido-bacillosamine biosynthesis in *C. jejuni* (Olivier et al. 2006). PglD has been shown to accept both GDP- and UDP-linked substrates, and as there is no evidence of bacillosamine

Table I. Bioinformatic analysis of candidate genes for CMP-Pse and CMP-Leg biosynthesis in *T. forsythia*

Strain locus tag	Best BLASTP match	Identity (%)	Bitscore	Known activity	Comments and references
ATCC 43037					
Tanf_01185	*H. pylori pseB* (HP0840)	56	355	4,6-Dehydratase/ 5-epimerase	McNally et al. (2008), Schoenhofen et al. (2006c)
Tanf_01190	*C. jejuni pseC* (Cj1294)	35	201	Aminotransferase	Schoenhofen et al. (2006a, 2006c)
Tanf_01215[a]	*C. jejuni pseH* (Cj1313)	34	60	N-acetyltransferase	Schoenhofen et al. (2006b)
Tanf_01235[a]	*C. jejuni pseG* (Cj1312)	27	70	UDP-sugar hydrolase	Contains PseG consensus sequence (Rangarajan et al. 2009, Schoenhofen et al. 2006b)
Tanf_01240	*H. pylori pseI* (HP0178)	49	332	Pseudaminic acid synthase	Chou et al. (2005)
Tanf_01200	*C. jejuni pseF* (Cj1311)	37	37	CMP-pseudaminic acid synthetase	Schoenhofen et al. (2006b)
92A2 / UB4					
BFO_1074	*C. jejuni legB* (Cj1319)	62	408	4,6-Dehydratase	Schoenhofen et al. (2009)
BFO_1073	*C. jejuni legC* (Cj1320)	49	385	Aminotransferase	Schoenhofen et al. (2009)
BFO_1067 [a]	*C. jejuni pglD* (Cj1123c)	30	83	N-acetyltransferase	Olivier et al. (2006), Schoenhofen et al. (2009)
BFO_1065	*C. jejuni legG* (Cj1328)	46	350	NDP-sugar hydrolase/ 2-epimerase	Member of NDP-N-acetylglucosamine 2-epimerase family (PFAM) (Schoenhofen et al. 2009)
BFO_1066	*C. jejuni legI* (Cj1327)	56	391	Legionaminic acid synthase	Schoenhofen et al. (2009)
BFO_1063	*C. jejuni legF* (Cj1331)	32	102	CMP-legionaminc acid synthetase	Schoenhofen et al. (2009)
BFO_1064	*C. jejuni ptmE* (Cj1329)	29	162	GlcN-1-P guanylyltransferase	Specific for GTP (Schoenhofen et al. 2009)

[a]Earlier start codon than in NCBI annotation.

occurring in *T. forsythia*, we propose that BFO_1067 is a dedicated part of the Leg biosynthesis pathway (i.e., LegH).

A phylogenetic comparison of NulO biosynthetic enzyme sequences by Lewis et al. (2009) indicated that NulO synthase sequences are better conserved than other NulO biosynthetic enzymes and, therefore, form the most conclusive basis for prediction of specific NulO sugar types in different organisms. Including *T. forsythia* sequences in this analysis, Tanf_01240 of the type strain ATCC 43037 is clustered in the phylogenetic clade of PseI enzymes, whereas BFO_1066 of strains FDC 92A2/UB4 shares ancestry with LegI sequences (Figure 3).

Biochemical characterization of a CMP-Pse biosynthetic locus in *T. forsythia* ATCC 43037

To confirm the role of the predicted Pse biosynthesis enzymes in the ATCC 43037 type strain, we recombinantly produced and characterized these proteins. PseB, PseH and PseI were expressed as His_6-tagged proteins in *E. coli* and purified by nickel-affinity chromatography (Figure 4A). In all three cases, C-terminal tags resulted in better protein expression and solubility than N-terminal tags. For PseC and PseG, a maltose-binding protein (MBP) fusion tag followed by purification over an amylose affinity column was used since, in these cases, the His_6-tagged constructs were found to be inactive. Subsequently, the enzymes were assayed for their ability to catalyze the various steps in the formation of CMP-Pse. The activity and product of each enzymatic step was confirmed by either capillary electrophoresis (CE) (Figure 5), CE–mass spectrometry (MS) (Supplementary Table I) or NMR spectroscopy (Table II). Starting with UDP-GlcNAc (I_P) as a precursor, PseB-His_6 was found to exhibit both C-4,6 dehydratase and C-5 epimerase activity that resulted in the production of UDP-2-acetamido-2,6-dideoxy-β-L-*arabino*-hexos-4-ulose (II_P). When the subsequent aminotransferase enzyme PseC-MBP was not present and this metabolite

was left to build up in overnight reactions, the formation of UDP-2-acetamido-2,6-dideoxy-α-D-*xylo*-hexos-4-ulose could be observed (data not shown), resulting from a further C5 epimerization of the *arabino*-4-keto Pse intermediate (II_P). This is characteristic of the PseB enzymes studied to date. Also, the addition of exogenous NAD^+ or $NADP^+$ did not improve reaction speed, indicating that sufficient cofactor was already tightly bound to the enzyme and recycled throughout catalysis. Identical properties have already been described for the *C. jejuni* PseB enzyme Cj1293 (Schoenhofen et al. 2006b). In the next step, a C-4 amino transfer of the 4-keto intermediate (II_P) forming UDP-4-amino-4,6-dideoxy-β-L-AltNAc (III_P) was accomplished by the aminotransferase PseC-MBP. PseH-His_6 was found to perform N-4 acetylation of III_P, forming UDP-2,4-diacetamido-2,4,6-trideoxy-β-L-altropyranose (IV_P). Next, 2,4-diacetamido-2,4,6-trideoxy-β-L-altropyranose (V_P) was formed by the removal of UDP from IV_P by the sugar hydrolase PseG-MBP. The condensation of V_P with pyruvate by PseI-His_6 created Pse5,7Ac_2 (VI_P). For the last enzyme of the pathway, CMP-Pse synthetase PseF, neither the His-tagged nor the MBP-fusion construct showed any activity on VI_p. However, using PseF from *H. pylori*, we were able to catalyze the activation of VI_P with CMP, forming CMP-Pse5,7Ac_2 (VII_P) (Figure 5; Table II). This finding might be indicative of the requirement of the 5Am7Gra modifications of Pse for activity of the *T. forsythia* PseF enzyme, or may simply indicate inactive enzyme due to in vitro tagging strategies (i.e., MalE- or His-tags). The former would also suggest possible relaxed specificity of enzymes PseB/C/ H/G/I, as we were able to produce Pse5,7Ac_2 with enzymes ultimately responsible for making Pse5Am7Gra. Importantly, the CMP-Pse5,7Ac_2 produced using Pse5,7Ac_2 prepared with *T. forsythia* enzymes was found to be identical to CMP-Pse5,7Ac2 previously characterized by NMR (Table II; Supplementary Figure 2). Our findings suggest that Pse biosynthesis in *T. forsythia* ATCC 43037 follows essentially the same biosynthetic route as in *C. jejuni* and *H. pylori* (Schoenhofen et al. 2006b).
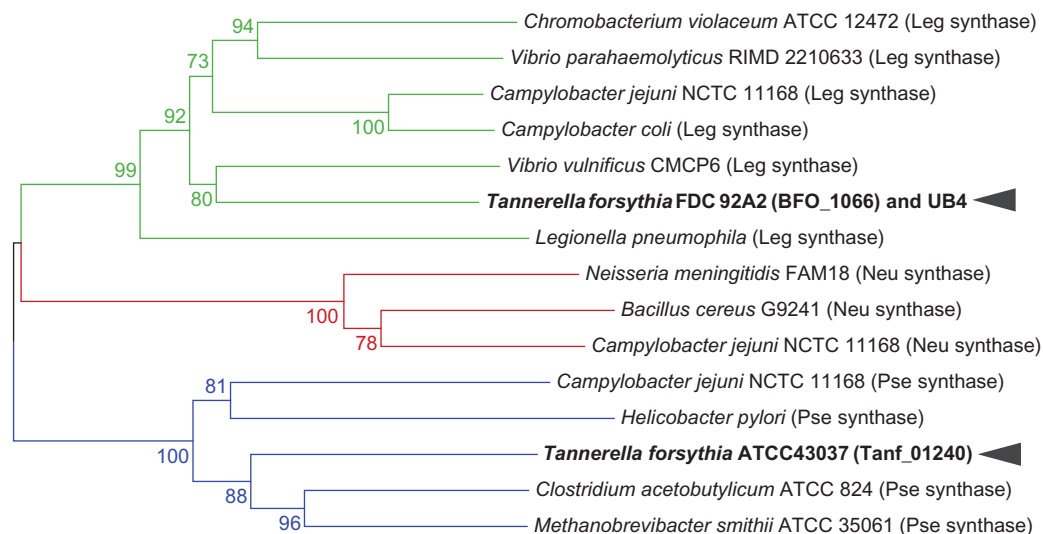
Fig. 3. Phylogenetic clusters of selected microbial NulO synthase homologs. Based on the prediction of NulO sugar type by Lewis et al. (2009), a distance-based neighbor joining tree calculated from the amino acid sequences of NulO synthase enzymes places Tanf_01240 of *T. forsythia* type strain ATCC 43037 in a phylogenetic clade of pseudaminic acid synthases, while BFO_1066 of strain FDC 92A2/UB4 is clustered with Leg synthases (bootstrap values shown at relevant nodes). Green denotes Leg synthases, red Neu synthases and blue Pse synthases. This figure is available in black and white in print and in color at *Glycobiology* online.
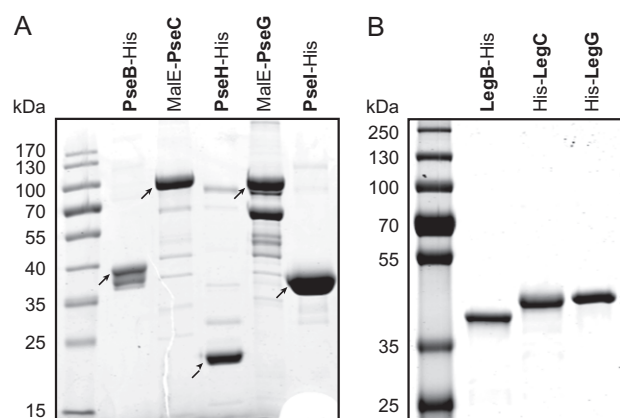

Fig. 4. SDS-PAGE gels (12%) of purified recombinant enzymes of the (**A**) CMP-Pse biosynthesis pathway from *T. forsythia* ATCC 43037 and (**B**) CMP-Leg biosynthesis pathway from *T. forsythia* FDC 92A2/UB4.

Biochemical characterization of the CMP-Leg biosynthesis locus in *T. forsythia* strains FDC 92A2/UB4

In contrast to the type strain, protein homology searches of the NulO biosynthesis gene locus in strains FDC 92A2/UB4 suggested a biosynthetic route towards Leg. To support this prediction, we conducted a series of functional characterizations of those biosynthetic enzymes that determine the stereochemical differences between the Pse and Leg pathway (Figure 2). For this purpose, BFO_1074 (*legB*), BFO_1073 (*legC*) and BFO_1065 (*legG*) were cloned and expressed in *E. coli*, and purified as His$_6$-tagged proteins (Figure 4B). Enzyme activity and reaction products were analyzed as described for strain ATCC 43037 above.

To substantiate the hypothesis that NulO biosynthesis in *T. forsythia* FDC 92A2/UB4 uses a GDP-linked precursor, we first assessed the substrate specificity of the first enzyme in the pathway, the LegB homolog BFO_1074 (Figure 6A). Since NAD(P)$^+$ is a necessary

cofactor for the C-4,6 dehydratase reaction, both NAD$^+$ and NADP$^+$ were added in separate reactions. Of all different nucleotide-activated GlcNAc-substrates that were used in our study (i.e., GDP-GlcNAc, UDP-GlcNAc (I$_P$), CDP-GlcNAc, dTDP-GlcNAc and IDP-GlcNAc), only GDP-GlcNAc (I$_L$) was converted by BFO_1074-His$_6$ (data only shown for UDP/GDP). Moreover, enough cofactor was bound to the purified enzyme to facilitate substrate conversion without any additional NAD(P)$^+$ present, albeit with slightly lower yields. In subsequent studies, we were able to determine that the reaction requires NAD$^+$ and does not use NADP$^+$ (data not shown), although increased conversion can even be seen for NAD-containing samples vs. NADP-containing ones (Figure 6A). The identity of the LegB-His$_6$ reaction product was confirmed by NMR (Table II) to be identical to the LegB product described in *C. jejuni*, which is GDP-2-acetamido-2,6-dideoxy-α-D-*xylo*-hexos-4-ulose (II$_L$). This finding marked a substantial difference to the Pse pathway as found in the type strain, where, in addition to the C-4,6 dehydration, epimerization at C-5 takes place.

Previous studies in *C. jejuni* have shown that the aminotransferases of the Pse, Leg and bacillosamine pathways display no cross-talk with their respective substrates, demonstrating the stereospecificity of each enzyme (Morrison and Imperiali 2014). Most importantly, *C. jejuni* LegC is absolutely specific for the GDP-4-keto intermediate formed by LegB. Overnight incubation of GDP-GlcNAc (I$_L$) with both BFO_1074-His$_6$ (LegB) and His$_6$-BFO_1073 (LegC) resulted in approximately 75% substrate conversion to GDP-4-amino-4,6-dideoxy-α-D-GlcNAc (III$_L$) (Figure 6B), the identity of which was again confirmed by NMR spectroscopy (Table II). Therefore, BFO_1073 can be considered a true LegC homolog that performs an equatorial addition of the amino group as opposed to the axial addition that PseC would catalyze (Figure 2). Lastly, the hydrolyzing 2-epimerase activity of BFO_1065 (putative LegG) was assayed. As with most of the enzymes of the *C. jejuni*-Leg pathway, *C. jejuni* LegG does not efficiently use the UDP-sugar precursor from the bacillosamine pathway, further reinforcing the specificity for a GDP-activated sugar (Schoenhofen et al. 2009; Morrison and Imperiali 2014). Since our attempts to express the putative
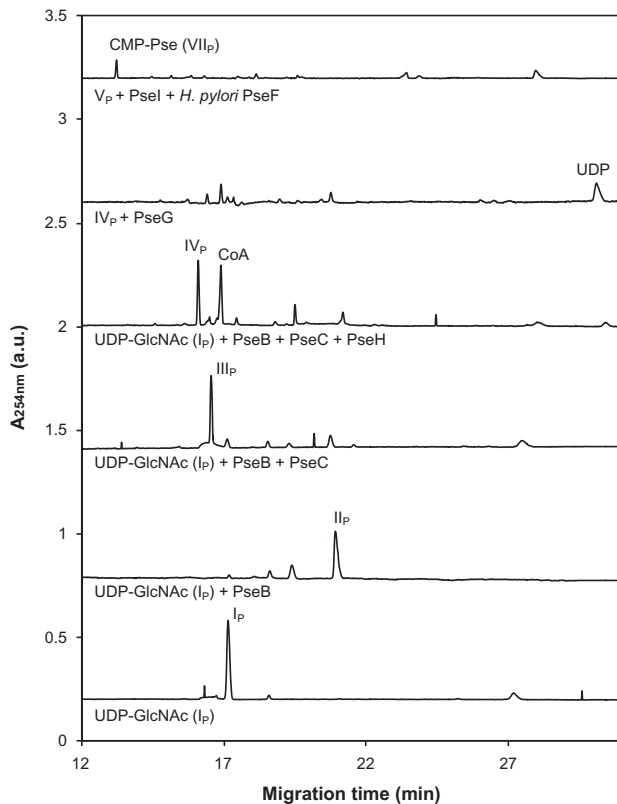
Fig. 5. CE analysis of the reaction products obtained by the incubation of UDP-GlcNAc (I_P) upon sequential addition of PseB-His$_6$, forming UDP-2-acetamido-2,6-dideoxy-β-L-*arabino*-hexos-4-ulose (II_P); PseC-MBP, forming UDP-4-amino-4,6-dideoxy-β-L-AltNAc (III_P); PseH-His$_6$, forming UDP-2,4-diacetamido-2,4,6-trideoxy-β-L-*altro*-pyranose (IV_P) and PseG-MBP, releasing UDP. Lastly, the combined action of PseI-His$_6$ and *H. pylori* PseF convert 2,4-diacetamido-2,4,6-trideoxy-β-L-*altro*-pyranose (V_P) via Pse5,7Ac$_2$ (VI_P) to CMP-Pse5,7Ac$_2$ (VII_P). Subscript "P" indicates intermediates from the CMP-Pse biosynthesis pathway.

N-acetyltransferase BFO_1067 failed, we used GDP-2,4-diacetamido-2,4,6-trideoxy-α-D-glucopyranose (IV_L) produced by *C. jejuni* LegH in our assay (Schoenhofen et al. 2009). Complete GDP removal and C-2 epimerization by His$_6$-BFO_1065 could be observed after just 15 min of incubation (Figure 6C; Table II), forming 2,4-diacetamido-2,4,6-trideoxy-D-mannopyranose (V_L). To note, due to lability of biosynthetic intermediates, a small amount of GDP is observed in control reactions lacking LegG. Our findings suggest that the NulO found in strains FDC 92A2/UB4 is a Leg derivative, and the biosynthetic pathway closely resembles that found in *C. jejuni* (Schoenhofen et al. 2009). This is in contrast to the Pse5Am7Gra NulO found in the type strain ATCC 43037 (Figure 1).

Construction and characterization of NulO-deficient *T. forsythia* strains

After having characterized both Pse and Leg biosynthesis pathways in vitro, the next step was the construction of knockout mutants deficient in the respective terminal NulO, thus facilitating the investigation of the enzymes' in vivo function and providing a valuable tool for future studies (Supplementary Figure 3). Since it was impossible to grow strain FDC 92A2 reliably, we used only strain UB4 for the creation of a Leg-deficient deletion mutant. The amplification and sequencing of various NulO biosynthesis genes indicated that

UB4 possesses the same Leg biosynthesis gene locus as strain FDC 92A2 (Supplementary Figure 4). This was confirmed by an alignment of the FDC 92A2 genome with the recently published genome of strain UB4, which revealed a nucleotide identity of 99.8% in this cluster (Stafford et al. in preparation). The aminotransferase genes *pseC* and *legC* were selected as targets for gene knockouts in the ATCC 43037 type strain and UB4, respectively. These were predicted to be specific and crucial to NulO synthesis and, therefore, result in a NulO-deficient background when deleted. To allow the identification of possible polar effects from the insertion of the knockout cassette, complementation mutants were also created.

As a first indication of altered S-layer glycan structure, sodium dodecyl sulfate-polyacrylamide gel electrophoresis (SDS-PAGE) analysis of *T. forsythia* ATCC 43037, UB4, and the respective NulO-deficient deletion mutants ATCC 43037 Δ*pseC* and UB4 Δ*legC* showed a clear downshift of the glycosylated S-layer proteins TfsA and TfsB (Figure 7). To analyze these changes in detail, in-gel reductive β-elimination was performed to release *O*-glycans for subsequent analysis by LC–electrospray ionization (ESI)–MS/MS (Supplementary Figure 5). With the ATCC 43037 wild-type glycan (1897.7 Da) serving as a reference, data from the ATCC 43037 Δ*pseC* knockout mutant were consistent with the loss of the terminal 379 Da Pse5Am7Gra residue (Table III). Moreover, we could observe the loss of a methyl group on the terminal *N*-acetylmannosaminuronic acid residue, while the MS/MS profile of the rest of the glycan remained unchanged (data not shown). Additional mass peaks corresponding to glycans lacking digitoxose, fucose, *N*-acetyl residues or combinations thereof are all in agreement with the previously published microheterogeneity of the *T. forsythia* oligosaccharide (Posch et al. 2011). In terms of overall sugar composition and glycan structure, the *O*-glycan of strain UB4 was found to be identical to that of ATCC 43037 apart from a −43 Da mass difference in the terminal trisaccharide branch. MS/MS data and analysis of glycan fragments indicated that the methyl group on the terminal *N*-acetyl-mannosaminuronic acid residue was missing (−14 Da), while the remaining mass defect of 29 Da could be attributed to a change in the terminal NulO (Table III; Supplementary Figure 5). Importantly, the S-layer glycan from a UB4 Δ*legC* knockout mutant was also found to be lacking a terminal NulO residue (Table III), specifically, a Leg derivative with a mass of 350 Da. In addition, we could consistently observe another glycan species with an additional +16 Da at the position of the digitoxose, indicating the presence of a deoxyhexose instead of a dideoxyhexose in some forms of the glycan.

Our data indicate that the Pse and Leg acid biosynthesis gene loci are functional and active in vivo and that strain UB4 carries a Leg residue with a different modification than the Pse in strain ATCC 43037, accounting for a mass difference of 29 Da. By way of calculation this could be explained by a change of the glyceroyl for a glycolyl and the acetimidyl for an acetyl group.

Analysis of biofilm formation of *T. forsythia* wild-type and NulO-deficient strains

To test a possible influence of the terminal NulO residue on biofilm growth, liquid cultures of *T. forsythia* parent strains, deletion mutants, and complemented strains were incubated in mucin-coated 24-well polysterene plates. The salivary glycoprotein mucin is heavily sialylated and has been shown to facilitate attachment and promote growth in the initial stages of biofilm formation in various oral bacteria including *T. forsythia* (Roy et al. 2011). After removal of planktonic cells, the OD_{600} of the resuspended biofilm was

Table II. NMR chemical shifts δ (ppm) for the pyranose rings of *T. forsythia* NulO biosynthesis intermediates analyzed in this study

| Compound		^{1}H	Literature δH (ppm)	Measured δH (ppm)	^{13}C	Literature δC (ppm)	Measured δC (ppm)
VII$_P$	CMP-pseudaminic acid (CMP-Pse5,7Ac$_2$)	H3$_{ax}$	1.60	1.60			
		H3$_{eq}$	2.22	2.21	C3	36.7	37.1
		H4	4.23	4.23	C4	65.5	66.1
		H5	4.28	4.28	C5	49.5	50.0
		H6	4.30	4.29	C6	73.4	73.9
		H7	4.02	4.02	C7	54.4	55.0
		H8	4.11	4.11	C8	69.4	69.9
		H9	1.20	1.19	C9	17.9	18.4
II$_L$	GDP-2-acetamido-2,6-dideoxy-α-D-*xylo*-hexos-4-ulose	H1	5.45	5.46	C1	95.3	95.5
		H2	4.10	4.09	C2	53.5	53.7
		H3	3.82	3.83	C3	72.4	72.5
		H5	4.11	4.11	C5	70.9	71.1
		H6	1.21	1.21	C6	12.4	12.5
III$_L$	GDP-4-amino-4,6-dideoxy-α-D-GlcNAc	H1	5.50	5.50	C1	95.6	95.5
		H2	4.06	4.06	C2	55.0	55.1
		H3	3.87	3.89	C3	69.1	69.0
		H4	2.96	2.99	C4	58.6	58.7
		H5	4.21	4.22	C5	68.0	67.9
		H6	1.32	1.32	C6	18.0	18.4
V$_L$	2,4-diacetamido-2,4,6-trideoxy-D-mannopyranose		α/β	α/β		α/β	α/β
		H1	5.11/4.96	5.11/4.97	C1	94.0/94.0	93.8/93.8
		H2	4.30/4.46	4.30/4.47	C2	53.8/54.8	53.8/54.7
		H3	4.06/3.84	4.08/3.85	C3	67.7/71.7	67.6/71.0
		H4	3.77/3.66	3.78/3.67	C4	54.8/54.5	54.6/54.3
		H5	3.97/3.51	3.98/3.52	C5	68.1/72.6	68.2/72.4
		H6	1.19/1.21	1.19/1.22	C6	18.0/18.0	18.0/18.0
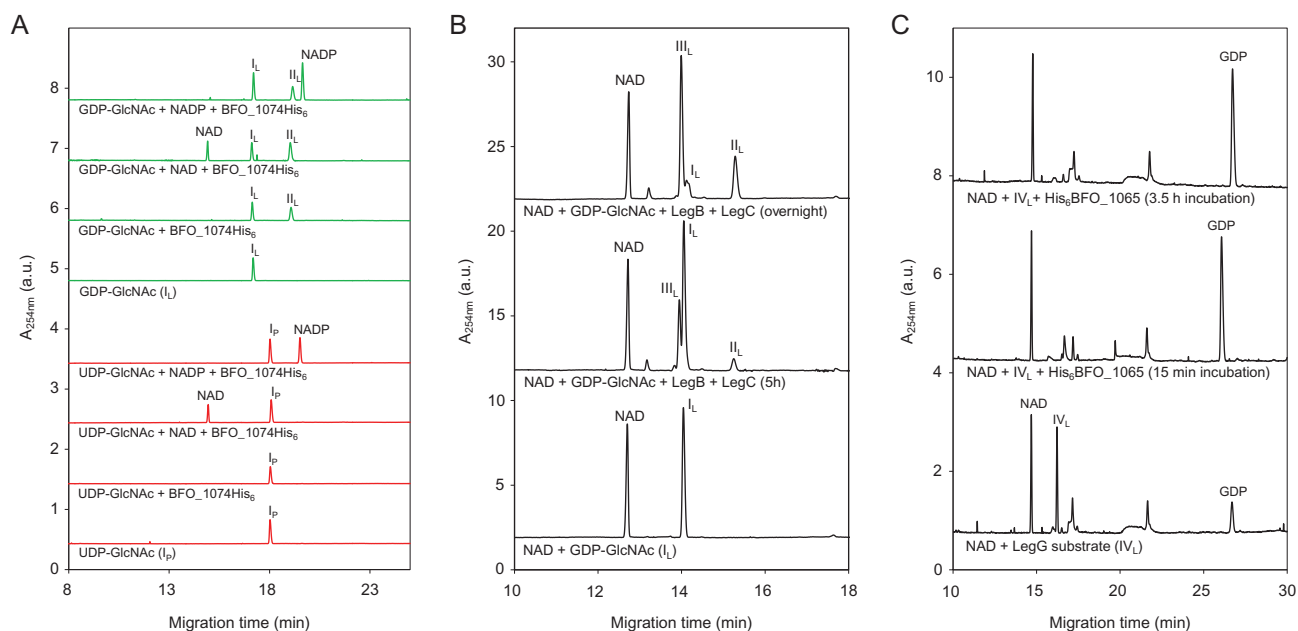
Fig. 6. CE analysis of the reaction products obtained by incubation of (**A**) BFO_1074-His$_6$ with UDP-GlcNAc (I$_P$, red traces) and GDP-GlcNAc (I$_L$, green traces) as substrate. Formation of product (GDP-2-acetamido-2,6-dideoxy-α-D-*xylo*-hexos-4-ulose (II$_L$)) could only be observed with GDP-GlcNAc (I$_L$), confirming that BFO_1074-His$_6$ is a LegB homolog that utilizes GDP-linked substrates. (**B**) GDP-GlcNAc (I$_L$) with both the dehydratase BFO_1074-His$_6$ (LegB) and the aminotransferase His$_6$-BFO_1073 (LegC), resulted in the formation of GDP-4-amino-4,6-dideoxy-α-D-GlcNAc (III$_L$). In the overnight reaction, a conversion of roughly 75% could be achieved. (**C**) GDP-2,4-diacetamido-2,4,6-trideoxy-α-D-glucopyrano (IV$_L$) with the hydrolyzing 2-epimerase BFO_1065 (LegG). Complete release of GDP from the substrate could be observed after 15 min of incubation. Subscripts "P" and "L" indicate intermediates from the CMP-Pse and CMP-Leg biosynthesis pathway, respectively. This figure is available in black and white in print and in color at *Glycobiology* online.
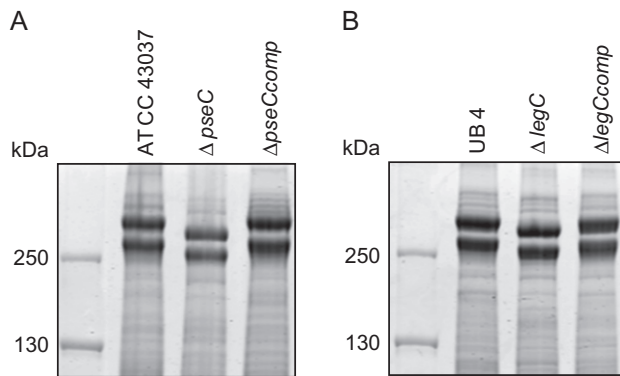
Fig. 7. SDS-PAGE analysis of *T. forsythia* parent, NulO-deficient, and complemented strains. (**A**) CBB stained SDS-PAGE (7.5% gel) of whole cell extracts from *T. forsythia* ATCC 43037, ATCC 43037 Δ*pseC* and the complemented strain ATCC 43037 Δ*pseC*comp, and (**B**) *T. forsythia* UB4 wild-type, UB4 Δ*legC* and the complemented strain UB4 Δ*legC*comp. For both *T. forsythia* ATCC 43037 Δ*pseC* and UB4 Δ*legC*, a downshift of the S-layer protein bands (TfsA and TfsB) could be observed, which was reverted in the complemented strains.

determined. Biofilm formation in the NulO-deficient mutants showed a 1.7-fold and 1.8-fold decrease for strain ATCC 43037 Δ*pseC* (Figure 8 A) and for UB4 Δ*legC* (Figure 8 B), respectively, when compared to the corresponding parent strain. In the complemented strains, biofilm formation was restored to the parent strains' levels, indicating that the decrease in biofilm growth is attributable to the loss of NulO biosynthesis rather than the insertion of a knockout cassette or the disruption of an operon.

Discussion

The purpose of this study was to examine the genetic and biochemical basis for the biosynthesis of the terminal, non-reducing end Pse derivative (Pse5Am7Gra) found on the S-layer *O*-glycan of *T. forsythia* ATCC 43037 (Posch et al. 2011). After discovering a strain misattribution in the publicly available genome of the type strain, we extended our investigation to strains FDC 92A2 and UB4. We have identified in three strains of *T. forsythia* distinct gene loci involved in the synthesis of the structurally distinct NulOs Pse or Leg. Through the subsequent characterization of the ATCC 43037 NulO biosynthetic enzymes, we could show their capability of producing CMP-Pse following the well-characterized UDP-sugar pathway of *H. pylori*, while the enzymes of strains FDC 92A2 and UB4 can follow the GDP-sugar route leading to CMP-Leg in *C. jejuni*. Considering the unique modifications of the NulOs in *T. forsythia* strains, however, it is likely that there might be deviations from the said pathways in vivo (Figure 2). Interestingly, a preliminary analysis of unpublished genomes found that a significantly higher number of the *T. forsythia* strains available to us contain the biosynthetic gene cluster for Leg than for Pse, suggesting that this type of NulO might be more prevalent than the one found in the type strain ATCC 43037. Whether the "equipment" of *T. forsythia* strains with Leg or Pse may reflect adaptations to specific oral microenvironments or is linked to the health status of the patients from which the isolates were derived remains elusive.

Despite testing both His6-tagged and MBP-fusion protein constructs, we were unable to detect activity for the last enzyme of the Pse pathway, the CMP-Pse synthetase PseF. While this can have several reasons, it is conceivable that at this stage of the pathway, PseF

can only process Pse that carries one or both of the modifications observed in the ATCC 43037 type strain (i.e., 5Am7Gra). Among NulO biosynthesis genes, sequence conservation between LegF and PseF homologs, respectively, is relatively low, which could indicate high specificity for a particularly modified substrate. Since knowledge about the identity and function of NulO-modifying enzymes is scarce, the elucidation of the biochemical mechanism and genetic basis for the *N*-acetimidoyl (Am) and *N*-glyceroyl (Gra) substitutions observed in the ATCC 43037 type strain remains a major challenge. In *Campylobacter spp.*, the Am- modifications of Pse and Leg appear to occur at the CMP-sugar stage (McNally et al. 2007). The genes involved in these substitutions (*pseA* and *ptmG* (*legA*), respectively) have been identified, but have no homolog in *T. forsythia* (data not shown). However, it may not be surprising that there is low similarity between a *T. forsythia* and a *C. jejuni* Am-modifying enzyme, since in *C. jejuni* the Am group is added to the C7 position of Pse, whereas in *T. forsythia* it is added to the C5 position. With regard to the Gra modification of Pse, the substitution of an *N*-acetyl (Ac) group of Pse by a 2,3-di-*O*-methyl glyceric acid residue has been described on the flagellin of *C. jejuni* 11168 (Logan et al. 2009). In *C. jejuni*, this Gra modification is found at C5, whereas in *T. forsythia* it is found at C7, and, again, may explain the inability to identify clear homologs between the two organisms. A glyceric acid residue at the C7 position of Pse has also been found in the LPS of *Vibrio vulnificus* (Vinogradov et al. 2009), but the responsible genes have yet to be identified.

While there are numerous reports of one distinct bacterium being capable of producing both Leg and Pse, variations of the NulO-type between strains of the same species have, to the best of our knowledge, so far only been described in *C. jejuni* (strain 81-176 only displays Pse derivatives, whereas strain 11168 displays Pse and Leg), *Campylobacter concisus* (Kaakoush et al. 2011), *Acinetobacter* spp. (Scott et al. 2014) and *Photobacterium profundum* (Lewis et al. 2009). The evolutionary purpose for such structural variation remains a matter of speculation. In *T. forsythia*, a likely driving force would be the development of sophisticated strategies for host evasion and virulence. It is conceivable that different NulO types play distinct roles in the molecular mimicry of host tissues, thus enabling the pathogen to avoid immune detection, modulate the host immune response and enter into host cells to escape immune surveillance (Amano et al. 2014). This may also suggest that some *T. forsythia* strains have a special "fit" with only certain hosts since NulO display is not a matter of turning gene content on or off but is fixed in their genomes—they are either displaying Pse or Leg at the cell surface. Owing to *T. forsythia*'s slow growth and recalcitrance to genetic manipulation, insights into the possible immunological function of the modified Pse in *T. forsythia* could so far only be derived from an ATCC 43037 Δ*wecC* deletion mutant (ED1 (Honma et al. 2007)) lacking the terminal trisaccharide motif of the S-layer glycan (comprised of two ManNAcA residues and the terminal Pse5Am7Gra; compare with Figure 1B; (Posch et al. 2011)). The Δ*wecC* mutant was found to induce significantly higher amounts of the pro-inflammatory cytokines IL-6, IL-1β and IL-23 secretion in mouse bone-marrow-derived dendritic cells and macrophages compared with *T. forsythia* parent cells. Moreover, the loss of that glycan motif rendered the pathogen increasingly prone to capture and killing by dendritic cells (Settem et al. 2013, 2014). In vivo, mice infected with the *T. forsythia* strain showed higher inflammatory alveolar bone loss than the Δ*wecC* mutant-infected mice, a consequence that could be attributed primarily to the parent-type's ability to activate TLR2, drive CD4+ T-cell differentiation toward Th2 whilst blocking Th17 and innate neutrophil

Table III. Overview of *T. forsythia* glycan species, detected *m/z* values, neutral masses and the anticipated mass of respective NulOs

Strain	Structure	*m/z* [M+H$^+$]$^+$	*m/z* [M+2H$^+$]$^{2+}$	Neutral mass [Da]	Neutral NulO mass [Da]	
					with linkage (-18 Da)	Full mass
ATCC 43037	*(glycan structure)*	1898.7	949.9	1897.7	361.14	379.15
ATCC 43037 Δ*pseC*	*(glycan structure)*	1523.4	762.3	1522.6	–	–
UB4	*(glycan structure)*	1855.6	928.3	1854.6	332.12	350.13
	(glycan structure, +16 Da)	1871.6	936.3	1870.6	332.12	350.13
UB4 Δ*legC*	*(glycan structure)*	1523.4	762.3	1522.6	–	–
	(glycan structure, +16 Da)	1539.4	770.3	1538.6	–	–

responses (Myneni et al. 2011; Settem et al. 2013). Although the Δ*wecC* mutant strain lacks three sugars instead of only just the Pse5Am7Gra residue, we speculate that the terminal NulO derivative plays the major role in the observed immunomodulatory effects, possibly through interactions with Siglec (sialic acid binding Ig-like lectin) receptors on immune cells. The deletion mutant Δ*pseC* created in the course of this study lacks only the terminal modified Pse and, therefore, represents a valuable tool for future studies in this direction. The analysis of *T. forsythia* UB4, a strain possessing the biosynthetic pathway for Leg, and its deletion mutant Δ*legC* revealed the presence of a NulO of unknown structure with a mass of 350 Da. A possible candidate that matches this mass requires an *N*-glycolyl (Gc) substitution at either C-5 or C-7, resulting in Leg5Ac7Gc or Leg5Gc7Ac. This modification is commonly found in the Sias of mammals in the form of the hydroxylated derivative of *N*-acetylneuraminic acid, Neu5Gc, but has, to the best of our knowledge, not yet been described in bacteria. The elucidation of the exact structure of the unknown NulO in *T. forsythia* UB4 using NMR spectroscopic methods will therefore be the main focus of future studies. Moreover, having identified different NulOs in the strains ATCC 43037 and UB4, in conjunction with our respective Δ*pseC* and Δ*legC* mutants, it is now possible to investigate the respective influence of Pse and Leg on Toll-like receptor 2 signaling and T-helper 17 responses.

As shown by our analysis of growth on mucin-coated microtiter plates, the knockout of *pseC* and *legC* in *T. forsythia* ATCC 43037 and UB4 cells, respectively, resulted in impaired biofilm formation as evidenced by a 1.7- (Δ*pseC*) and 1.8-fold (Δ*legC*) decrease compared to the parent strains. In either case biofilm formation could be fully restored in the respective complemented mutant (Figure 8), indicating that NulO loss directly correlates with reduced biofilm formation. For comparison, the *T. forsythia* ATCC 43037 Δ*wecC* mutant for which enhanced biofilm formation had been reported previously (Honma et al. 2007), was included in our study. Interestingly, in our microtiter assay, this mutant exhibited a 3.6-fold decrease in biofilm formation compared to the parent strain (data not shown). This discrepancy of our and previous data might be explained by the different surface characteristics of the plates used in the assays. In our
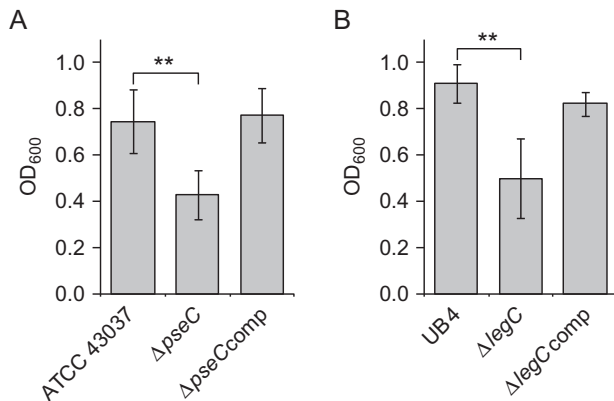
study, mucin was used to foster the biofilm formation (Roy et al. 2011, 2012), since apart from facilitating initial attachment and promoting growth, coating of the plates with this glycoprotein also confers highly hydrophilic properties to the inherent hydrophobic polystyrene surfaces (Crouzier et al. 2013) and simultaneously mirrors the native habitat of the bacterium. Thus, it is conceivable that a Δ*wecC* mutant (lacking three charged sugar residues) exhibits reduced biofilm formation when grown on hydrophilic surface, while the comparably more hydrophobic, non-coated polystyrene plates might have favored the opposite. Furthermore, a study of a deletion mutant of the OmpA-like protein (Tanf_10935/TF1331) showed that this knockout resulted in a significant reduction of cell surface hydrophobicity and biofilm-forming activity on hydrophobic polystyrene plates (Abe et al. 2011). Both these findings are in agreement with our results and support the hypothesis that the surface of the plates, when rendered from hydrophobic to hydrophilic, causes a decrease of biofilm formation in strains such as Δ*wecC* (Honma et al. 2007; Posch et al. 2011), Δ*pseC* and Δ*legC* (this study) that lack one or more charged residues.

In summary, our findings contribute to the understanding of the biosynthesis of two distinct NulOs in two strains of the same species and provide valuable tools for the investigation of the biofilm lifestyle and the immunogenic potential of *T. forsythia*. Considering the likely involvement of this pathogen's NulOs in the modulation of immune responses and the increasing reports of Sia-like sugars being linked to bacterial pathogenesis (Figure 9), future experiments will be aimed at elucidating the mechanisms that govern the interactions of *T. forsythia* with the host as well as other bacteria of the oral microflora. Ultimately, these insights will facilitate the development of future strategies to control periodontal disease.

Fig. 8. Knockout of *pseC* and *legC* decreases biofilm formation of *T. forsythia* ATCC 43037 and *T. forsythia* UB4 cells, respectively. (**A**) Biofilm formation in *T. forsythia* ATCC 43037 wild-type compared to ATCC 43037 Δ*pseC* and the complemented strain ATCC 43037 Δ*pseC*comp. (**B**) Biofilm formation in *T. forsythia* UB4 wild-type compared to UB4 Δ*legC* and the complemented strain *T. forsythia* UB4 Δ*legC*comp. Data represent mean values ± SD of at least four independent experiments with four replicates each and were analyzed by the unpaired Student's *t*-test. Asterisks indicate significant differences (**$P < 0.01$).

Materials and methods

Strains and culture conditions

T. forsythia ATCC 43037 (American Type Culture Collection, Manassas, VA), *T. forsythia* FDC 92A2 (obtained from Dr. Graham Stafford, University of Sheffield, UK) and *T. forsythia* UB4 (obtained
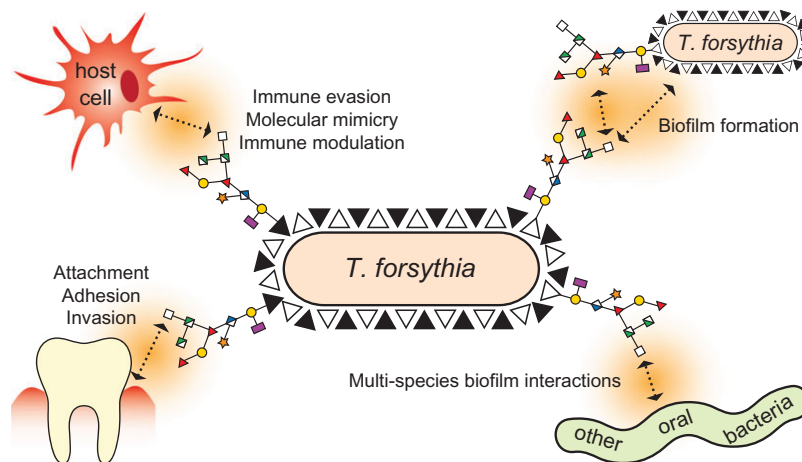

Fig. 9. Possible biological roles of the NulOs of the *T. forsythia* S-layer glycan. Representing the terminal sugars on the outermost surface structure of *T. forsythia* strains, Pse or Leg could have several functions. As previous studies have found the terminal trisaccharide of the S-layer glycan to be involved in the modulation of cytokine release and the suppression of Th17 responses, we hypothesize that the different NulOs displayed by *T. forsythia* strains are implicated in this phenomenon. Apart from the effect on monospecies biofilm formation described in this paper, the terminal NulOs are likely to play a role in the bacterium's interactions with other species of the subgingival microbiota. Furthermore, they could exert an influence on how the bacterium attaches to periodontal surfaces and how it invades host tissue. The variation of the NulO type among various *T. forsythia* strains may reflect a special 'fit' with only certain hosts and/or microenvironments. This figure is available in black and white in print and in color at *Glycobiology* online.

from Dr. Ashu Sharma, University of Buffalo, NY) and the knockout mutants were grown anaerobically at 37 °C for 4–7 days in brain heart infusion (BHI) broth or 0.8% (w/v) BHI agar, supplemented with *N*-acetylmuramic acid and horse serum as described previously ([Tomek et al. 2014](#)). And 5 g/ml erythromycin (Erm), 10 μg/ml chloramphenicol (Cat) and 50 μg/ml gentamycin (Gent) were added when appropriate. *Escherichia coli* DH5α (Invitrogen), *E. coli* BL21 (DE3) (Invitrogen) and *E. coli* BL21-CodonPlus [DE3]-RIL (Novagen) cells were cultivated at 37°C and 200 rpm in lysogeny broth (LB) medium or 2xYT medium (16 g/l tryptone, 10 g/l yeast extract, 5 g/L NaCl) optionally supplemented with 100 μg/ml ampicillin (Amp), 50 μg/ml kanamycin (Km) or 30 μg/ml chloramphenicol (Cm), respectively. All strains used in this study are listed in Supplementary Table II.

DNA techniques and plasmid construction

All enzymes were purchased from Thermo Scientific. Genomic DNA of *T. forsythia* was isolated from 2 ml of bacterial suspension as described previously ([Cheng and Jiang 2006](#)). The GeneJET™ Gel Extraction Kit (Fermentas) was used to purify DNA fragments from agarose gels and to purify digested plasmids and oligonucleotides. Plasmid DNA from transformed cells was isolated with the GeneJET™ Plasmid Miniprep kit (Fermentas). Primers for PCR and DNA sequencing were purchased from Invitrogen (Supplementary Table III). PCR was performed using the Phusion® High-Fidelity DNA Polymerase (Fermentas) and the thermal cycler My CyclerTM (Bio-Rad). For recombinant expression in *E. coli* BL21 (DE) cells, plasmids encoding PseB, PseH and PseI were created as C-terminal His$_6$-tag fusion constructs by PCR using *T. forsythia* ATCC 43037 genomic DNA as a template and the primers 11/12, 28/22 and 33/34, respectively. The His$_6$-tagged amplification products were digested with NcoI/XhoI (*pseB* and *pseH*) and BsaI/XhoI (*pseI*), and all were cloned into NcoI/XhoI-linearized pET28a(+) (Novagen). PseC, PseG and PseH were produced as N-terminal MBP fusion proteins. After amplification using the primers 80/86, 81/105 and 101/102, respectively, the amplicons were digested with BamHI/HindIII and cloned into BamHI/HindIII-linearized pMAL_c2E vector (NEB). Plasmids encoding the Leg biosynthetic enzymes of strain FDC 92A2 were constructed as C-terminal (LegB) and N-terminal (LegC and LegG) His$_6$-tagged fusion constructs, after having the genes synthesized (Life Technologies). To overcome problems with low expression, *legG* was codon-optimized for *E. coli*. The synthesized gene sequences were amplified using the primers V83/84, V133/134 and V114/115, used for blunt-ended ligations into pCR2.1 and subsequently cloned into pET22b via NdeI/XhoI.

Transformation of chemically competent *E. coli* DH5α, *E. coli* BL21 (DE3) and *E. coli* BL21-CodonPlus[DE3]-RIL (Novagen) cells was performed according to the manufacturer's protocols. Transformants were screened by PCR using RedTaq ReadyMix PCR mix (Sigma-Aldrich), and recombinant clones were analyzed by restriction mapping and confirmed by sequencing (Microsynth).

His$_6$-tagged protein expression and purification

The plasmids encoding the Pse biosynthesis enzymes (pET28a_pseB, pMAL_2cE_pseC, pET28a_pseH, pMAL_2cE_pseG, pET28a_pseI and pMAL_2cE_pseH) were transformed into *E. coli* BL21 (DE3) cells, while those encoding biosynthesis enzymes of the Leg pathway (TF2074N-pet22b, TF2075C-pet22b and BFO_1065N-pet22b) were expressed in *E. coli* BL21-CodonPlus[DE3]-RIL. Freshly transformed cells were grown in LB or 2xYT medium to the mid-exponential

growth phase (OD$_{600}$ ~0.6) and protein expression was induced with a final concentration of 0.5 mM (Pse enzymes) or 0.1 mM (Leg enzymes) isopropyl-β-D-thiogalactopyranosid (IPTG). Cultures were grown for an additional 4 h at 37 °C and 200 rpm (PseG and PseH), were put on ice for 20 min and incubated overnight at 22 °C (PseB, PseC, PseI, PseF) or were incubated for 3 h at 30 °C (LegB, LegC and LegG). Cells were harvested by centrifugation (4500 × *g*, 30 min, 4 °C).

For purification of His$_6$-tagged enzymes, the cell pellets were resuspended in lysis buffer (50 mM sodium phosphate, pH 7.3, 400 mM NaCl, 10 mM β-mercaptoethanol) containing 10 mM imidazole, 10 μg/ml of DNaseI (Roche Applied Science) and EDTA-free protease inhibitor mixture (cOmplete, Roche Applied Science). The cells were disrupted by two passes through a French pressure cell (Amicorp) or an emulsiflex C5 (20,000 psi). Lysates were centrifuged at 100,000 × *g* for 50 min at 4 °C, and the supernatant fraction was applied to a 3-ml nickel–nitrilotriacetic acid (Qiagen) column equilibrated in lysis buffer using a flow rate of 1 ml/min. After sample application, the column was washed with eight column volumes of lysis buffer. To elute the protein of interest, a linear gradient from 10 to 100 mM imidazole in lysis buffer was applied over 14 column volumes prior to a final pulse of 14 column volumes of 200 mM imidazole in lysis buffer. MBP-fusion proteins were purified according to the manufacturer's protocol using 2-ml amylose resin (NEB) per litre of culture. Fractions containing the purified protein of interest, as determined by SDS-PAGE (12.5%) upon Coomassie Brilliant Blue G250 (CBB) staining, were pooled and dialyzed against dialysis buffer (25 mM sodium phosphate, 25 mM NaCl, pH 7.3) overnight at 4 °C. Protein concentration was measured spectrophotometrically and calculated using A$_{280}$ 0.1% values obtained from the exPASy ProtParam tool (http://web.expasy.org/protparam).

Enzymatic assays

Enzymatic assays and metabolite/product purification was performed similarly to methods described previously ([Schoenhofen et al. 2006b](#); [Schoenhofen et al. 2009](#); [Gulati et al. 2015](#)). Typically, NulO biosynthetic pathway reactions were performed at 37 °C in 25 mM sodium phosphate pH 7.3–7.8, 25 mM NaCl with 1 mM NDP-GlcNAc, 0.5 mM NAD$^+$ or NADP$^+$, 10 mM L-Glu, 0.5 mM PLP, 1.2 mM acetyl-CoA, 1.2 mM PEP and 2 mM MgCl$_2$ as necessary. CMP-activation of Pse5,7Ac$_2$ was performed using a CMP-pseudaminic acid synthetase, PseF, from *H. pylori* ([Schoenhofen et al. 2006a](#) Glycobiology). Reactions contained 50 mM Tris/HCl pH 9, 50 mM MgCl$_2$, 0.5 mM CTP, ~0.5 mM Pse5,7Ac$_2$, and sufficient quantities of pyrophosphatase as well as PseF.

Detection of Pse/Leg pathway biosynthetic genes in *T. forsythia* ATCC 43037, FDC 92A2 and UB4

To check for the presence of selected genes from the Pse or Leg biosynthesis pathway, genomic DNA of *T. forsythia* ATCC 43037, *T. forsythia* FDC 92A2 and *T. forsythia* UB4 was used as a template in six separate PCRs. Primers 11/12, 80/86 and 23/24 were used to amplify *pseB*, *pseC* and *pseF* of the Pse biosynthesis pathway. Primers V83/84, V26/27 and V63/64 were used to amplify *legB*, *legC* and *legF* of the Leg biosynthesis pathway. Amplification products of the UB4 strain were sequenced to confirm identity to the sequenced genome of strain FDC 92A2.

Gene knockouts

The gene knockout cassette used for constructing the *T. forsythia* ATCC 43037 Δ*pseC* and UB4 Δ*legC* mutants consisted of a 1093-base-pair (bp) Erm resistance gene P(ermF)_ermF flanked by homologous upstream and downstream regions. The ~1000-bp upstream and ~1000-bp downstream homology regions of the *pseC* gene (Tanf_01190) and of the *legC* gene (BFO_1073) were amplified from genomic DNA of *T. forsythia* ATCC 43037 and *T. forsythia* UB4, respectively, using the primers 5/6 (ATCC upstream), 7/8 (ATCC downstream), 88/89 (UB4 upstream) and 90/91 (UB4 downstream), respectively. The 1093-bp Erm resistance gene P(ermF)_ermF was amplified from genomic DNA of *T. forsythia* Δ*wecC* (obtained from A. Sharma, State University of New York at Buffalo, NY) using the primers 1 and 2. The three fragments were joined by overlap extension (OE-) PCR and sub-cloned into the blunt-end cloning vector pJET1.2 (Thermo Scientific). The corresponding plasmids were named pJET1.2_pseC_ermF and pJET1.2_legC_ermF. Transformation of *T. forsythia* ATCC and *T. forsythia* UB4 was done as described previously (Tomek et al. 2014, Megson et al. 2015). Cells were regenerated in BHI medium for 24 h before plating on BHI agar plates containing Erm as selection marker. Single colonies were picked and used for inoculation of liquid BHI medium. Once bacterial growth was visible, genomic DNA was isolated to confirm the integration of the knockout cassette via PCR amplification. The upstream and downstream integration as well as the loss of the gene were checked, using the primers 38/3 (ATCC upstream), 4/10 (ATCC downstream), 15/18 (ATCC loss of gene), 92/3 (UB4 upstream), 4/93 (UB4 downstream) and V26/V27 (UB4 loss of gene), respectively.

The complementation cassette for *T. forsythia* mutants consisted of a 651-bp Cm resistance gene flanked by a homologous ~1000-bp upstream region, the gene of interest and a ~1000-bp downstream region. The Cm resistance gene was amplified containing KpnI/SphI restriction sites at the C-terminus from the pEXALV vector (Zarschler et al. 2009) using the primers 75/77. The ~1000-bp upstream region plus the gene of interest, and the ~1000-bp downstream homology regions containing also the two restriction sites were amplified from genomic DNA of *T. forsythia* ATCC 43037 or *T. forsythia* UB4, using the primers 5/46 (ATCC upstream), 78/79 (ATCC downstream), 88/86 (UB4 upstream) and 94/95 (UB4 downstream), respectively. The ~1000-bp upstream region plus the gene of interest and the Cm resistance gene were joined by overlap extension (OE-) PCR and sub-cloned into the blunt-end cloning vector pJET1.2 (Thermo Scientific) resulting in plasmids pJET1.2_pseC_up+gene_cat and pJET1.2_legC_up+gene_cat. The ~1000-bp downstream homology regions were cloned into pJET1.2_pseC_up+gene_cat and pJET1.2_ legC_up+gene_cat using the KpnI and SphI restriction sites. The corresponding plasmids were named pJET1.2_pseC_cat and pJET1.2_legC_cat. Transformation of *T. forsythia* ATCC Δ*pseC* and *T. forsythia* UB4 Δ*legC* was done as described previously (Tomek et al. 2014; Megson et al. 2015).

CE analysis

CE analysis was performed using a P/ACE MDQ system (Beckman Instruments) with diode array detection. The running buffer was 25 mM sodium tetraborate, pH 9.4. The capillary was bare silica 50 μm × 50 cm, with a detector at 50 cm. The capillary was conditioned before each run by washing with 0.2 M NaOH for 2 min, water for 2 min, and running buffer for 2 min. Samples were introduced by pressure injection for 6 s, and the separation was performed at 18 kV for 20–30 min. Peak integration was done using the Beckman P/ACE station software.

Capillary electrophoresis–mass spectrometry

Separation of ions was achieved by CE (Prince CE system (Prince Technologies, Netherlands)) in a 90-cm long bare fused-silica capillary (365 μm OD × 50 μm ID). The 30 mM morpholine aqueous running CE buffer (adjusted to pH 9 with formic acid) was coupled with the capillary sheath fluid (isopropanol:methanol [2:1]) at their interface prior to MS (API3000 mass spectrometer [Applied Biosystems/Sciex, Concord, ON, Canada]).

NMR spectroscopy

For structural characterization of NulO pathway intermediates, filtered enzymatic reactions (Amicon Ultra-4 centrifugal filter unit with 3000 kDa molecular weight cut-off) or material purified according to previously described methods was exchanged into 100% D_2O (Gulati et al. 2015). Structural analysis was performed using either a Varian Inova 500 MHz (^{1}H) spectrometer with a Varian Z-gradient 3-mm probe or a Varian 600 MHz (^{1}H) spectrometer with a Varian 5 mm Z-gradient probe. All spectra were referenced to an internal acetone standard (δ_H 2.225 ppm and δ_C 31.07 ppm).

Mass spectrometric glycan structure analysis

For the analysis of the glycan structure in *T. forsythia* strains and mutants, S-layer *O*-glycans were released from purified TfsA S-layer protein by in-gel reductive β-elimination (Posch et al. 2011). The excised gel slices were covered with 1.0 M NaBH4 in 0.5 M NaOH and incubated at 50 °C overnight. Excess salt was removed with porous graphitic carbon (PGC) solid phase extraction cartridges (HyperSep-96- Hypercarb, 25 mg, Thermo Scientific). Briefly, the cartridges were equilibrated with 500 μl of 60% acetonitrile and washed three times with 500 μl water. Sample was added and washed twice with water. Reduced glycans were eluted using 350 μl 60% acetonitrile, vacuum dried and taken up in water. *O*-glycans were then analyzed by LC–ESI–MS/MS on a Hypercarb PGC column (100 × 0.32 mm, 5 μm pore size, Thermo Scientific) with a 20-min gradient from 1 to 28% acetonitrile in formate buffer of pH 3.0 at a flow rate of 6 μl/min using an Ultimate 3000 capillary flow LC (Dionex). Eluted glycans were registered on a Bruker amaZon ion trap using ESI and data dependent acquisition. Qualitative evaluation was done using Bruker's Data Analysis 4.0, where the all spectra within the relevant elution range were summed up to generate an average spectrum. The glycan nature of the main peaks was confirmed by the identification of specific reporter ions in MS/MS spectra, which was done by the help of Glycoworkbench 2.0 (Ceroni et al. 2008).

Biofilm microtiter plate assay

The ability of the different *T. forsythia* strains and NulO mutants to form biofilm on an abiotic surface was evaluated according to Roy et al. (2011). Cultures were grown for 2–3 d in half-concentrated BHI medium, diluted to an OD_{600} ~0.05 with sterile nutrient medium, and 1-ml aliquots were transferred into 24-well polystyrene plates (STARLAB) that were coated overnight at 37 °C with 500 μl of mucin (from bovine submaxillary gland, Sigma-Aldrich) solution (0.5 mg/ml in 0.1 M sodium acetate buffer pH 4.5). As a control, sterile nutrient medium was used. Cultures were incubated under anaerobic conditions at 37°C for 3 d (*T. forsythia* ATCC 43037, ATCC 43037 Δ*pseC* and ATCC 43037 Δ*pse*Ccomp) or 6 d (*T. forsythia* UB4, *T. forsythia* UB4 Δ*legC* and *T. forsythia* UB4 Δ*leg*Ccomp) without shaking. Two wells of each sample were used to determine the total optical density of the strains for later

normalization. Subsequently, planktonic cells were gently removed with a pipette and the plates were washed once with PBS buffer. Cells were resuspended in 1 ml of PBS buffer and the OD_{600} of the biofilm was determined. Biofilm values were normalized to the corresponding absorbance of the total biofilm. Data represent mean values $\pm$ SD of at least four independent experiments with four replicates each and were analyzed by the unpaired Student's *t*-test. Asterisks indicate significant differences ($*P < 0.05$; $**P < 0.01$; $***P < 0.001$).

Supplementary data

Supplementary data are available at *Glycobiology* online.

Funding

Acknowledgements

Conflict of interest statement

None declared.

Abbreviations

Ac, *N*-acetyl or acetamido; Am, *N*-acetimidoyl or acetamidino; Amp, ampicillin; AltNAc, *N*-acetyl-β-L-altrosamine; BLASTP, protein-protein Basic Local Alignment Search Tool; BHI, brain heart infusion; Cat, chloramphenicol; CBB, Coomassie Brilliant Blue G250; CDP, cytidine-5′-diphosphate; CE, capillary electrophoresis; Cm, chloramphenicol; CMP, cytidine-5′-monophosphate; CoA, coenzyme A; CTP, cytidine-5′-triphosphate; dTDP, 2′-deoxythymidine-5′-diphosphate; Erm, erythromycin; ESI, electrospray ionization; Fo, *N*-formyl; Gc, *N*-glycolyl; GDP, guanosine-5′-diphosphate; Gent, gentamycin; GlcN, glucosamine; GlcNAc, *N*-acetyl glucosamine; Glu, glutamate; Gra, *N*-glyceroyl or *N*-2,3-dihydroxypropionyl or glycerate group; Hb, *N*-hydroxybutyryl; IDP, inosine-5′-diphosphate; IL, interleukin; IPTG, isopropyl-β-D-thiogalactopyranosid; Km, kanamycin; LB, lysogeny broth; LC, liquid chromatography; Leg, legionaminic acid ($Leg5,7Ac_2$), 5,7-diacetamido-3,5,7,9-tetradeoxy-D-*glycero*-D-*galacto*-nonulosonic acid; LPS, lipopolysaccharide; MBP, maltose-binding protein; MS, mass spectrometry; NAD^+, nicotinamide adenine dinucleotide; $NADP^+$, nicotinamide adenine dinucleotide phosphate; NDP, nucleotide diphosphate; Neu, neuraminic acid; NMR, nuclear magnetic resonance; NulO, nonulosonic acid; ORF, open reading frame; PBS, phosphate-buffered-saline; PEP, phosphoenolpyruvate; PGC, porous graphitic carbon; P_i, inorganic phosphate; PLP, pyridoxal-5′-phosphate; PPi, pyrophosphate; Pse, pseudaminic acid ($Pse5,7Ac_2$), 5,7-diacetamido-3,5,7,9-tetradeoxy-L-*glycero*-L-*manno*-nonulosonic acid; SDS-PAGE, sodium dodecyl sulfate-polyacrylamide gel electrophoresis; Sia, sialic acid (Neu5Ac), 5-acetamido-3,5-dideoxy-D-*glycero*-D-*galacto*-nonulosonic acid; Siglec, sialic acid binding Ig-like lectin; Th, T helper cell; TLR2, toll-like receptor 2; UDP, uridine-5′-diphosphate

References

Abe T, Murakami Y, Nagano K, Hasegawa Y, Moriguchi K, Ohno N, Shimozato K, Yoshimura F. 2011. OmpA-like protein influences cell shape and adhesive activity of *Tannerella forsythia*. Mol Oral Microbiol. 26:374–387.

Amano A, Chen C, Honma K, Li C, Settem RP, Sharma A. 2014. Genetic characteristics and pathogenic mechanisms of periodontal pathogens. *Adv Dent Res*. 26:15–22.

Carlin AF, Uchiyama S, Chang YC, Lewis AL, Nizet V, Varki A. 2009. Molecular mimicry of host sialylated glycans allows a bacterial pathogen to engage neutrophil Siglec-9 and dampen the innate immune response. *Blood*. 113:3333–3336.

Ceroni A, Maass K, Geyer H, Geyer R, Dell A, Haslam SM. 2008. GlycoWorkbench: A tool for the computer-assisted annotation of mass spectra of glycans. *J Proteome Res*. 7:1650–1659.

Cheng HR, Jiang N. 2006. Extremely rapid extraction of DNA from bacteria and yeasts. *Biotechnol Lett*. 28:55–59.

Chou WK, Dick S, Wakarchuk WW, Tanner ME. 2005. Identification and characterization of NeuB3 from *Campylobacter jejuni* as a pseudaminic acid synthase. *J Biol Chem*. 280:35922–35928.

Crouzier T, Jang H, Ahn J, Stocker R, Ribbeck K. 2013. Cell patterning with mucin biopolymers. *Biomacromolecules*. 14:3010–3016.

Darveau RP. 2010. Periodontitis: A polymicrobial disruption of host homeostasis. *Nat Rev Microbiol*. 8:481–490.

Edebrink P, Jansson PE, Bogwald J, Hoffman J. 1996. Structural studies of the *Vibrio salmonicida* lipopolysaccharide. *Carbohydr Res*. 287:225–245.

Fagan RP, Fairweather NF. 2014. Biogenesis and functions of bacterial S-layers. *Nat Rev Microbiol*. 12:211–222.

Friedrich V, Pabinger S, Chen T, Messner P, Dewhirst FE, Schäffer C. 2015. Draft genome sequence of *Tannerella forsythia* type strain ATCC 43037. *Genome Announc*. 3:e00660–15.

Guerry P, Ewing CP, Schirm M, Lorenzo M, Kelly J, Pattarini D, Majam G, Thibault P, Logan S. 2006. Changes in flagellin glycosylation affect *Campylobacter* autoagglutination and virulence. *Mol Microbiol*. 60:299–311.

Gulati S, Schoenhofen IC, Whitfield DM, Cox AD, Li J, St Michael F, Vinogradov EV, Stupak J, Zheng B, Ohnishi M, et al. 2015. Utilizing CMP-sialic acid analogs to unravel *Neisseria gonorrhoeae* lipooligosaccharide-mediated complement resistance and design novel therapeutics. *PLoS Pathog*. 11:e1005290.

Hajishengallis G, Lamont RJ. 2012. Beyond the red complex and into more complexity: The polymicrobial synergy and dysbiosis (PSD) model of periodontal disease etiology. *Mol Oral Microbiol*. 27:409–419.

Haseley SR, Wilkinson SG. 1997. Structural studies of the putative O-specific polysaccharide of *Acinetobacter baumannii* O24 containing 5,7-diamino-3,5,7,9-tetradeoxy-L-*glycero*-D-*galacto*-nonulosonic acid. *Eur J Biochem*. 250:617–623.

Holt SC, Ebersole JL. 2005. *Porphyromonas gingivalis*, *Treponema denticola*, and *Tannerella forsythia*: The "red complex", a prototype polybacterial pathogenic consortium in periodontitis. *Periodontol 2000*. 38:72–122.

Honma K, Inagaki S, Okuda K, Kuramitsu HK, Sharma A. 2007. Role of a *Tannerella forsythia* exopolysaccharide synthesis operon in biofilm development. *Microb Pathog*. 42:156–166.

Horzempa J, Dean CR, Goldberg JB, Castric P. 2006. *Pseudomonas aeruginosa* 1244 pilin glycosylation: Glycan substrate recognition. *J Bacteriol*. 188:4244–4252.

Howard SL, Jagannathan A, Soo EC, Hui JP, Aubry AJ, Ahmed I, Karlyshev A, Kelly JF, Jones MA, Stevens MP, et al. 2009. *Campylobacter jejuni* glycosylation island important in cell charge, legionaminic acid biosynthesis, and colonization of chickens. *Infect Immun*. 77:2544–2556.

Kaakoush NO, Deshpande NP, Wilkins MR, Raftery MJ, Janitz K, Mitchell H. 2011. Comparative analyses of *Campylobacter concisus* strains reveal the genome of the reference strain BAA-1457 is not representative of the species. *Gut Pathog*. 3:15.

Kenyon JJ, Marzaioli AM, De Castro C, Hall RM. 2015. 5,7-di-N-acetyl-acinetaminic acid: A novel non-2-ulosonic acid found in the capsule of an *Acinetobacter baumannii* isolate. *Glycobiology*. 25:644–654.

Kenyon JJ, Marzaioli AM, Hall RM, De Castro C. 2014. Structure of the K2 capsule associated with the KL2 gene cluster of *Acinetobacter baumannii*. *Glycobiology*. 24:554–563.

Kiss E, Kereszt A, Barta F, Stephens S, Reuhs BL, Kondorosi A, Putnoky P. 2001. The rkp-3 gene region of *Sinorhizobium meliloti* Rm41 contains strain-specific genes that determine K antigen structure. *Mol Plant Microbe Interact*. 14:1395–1403.

Knirel YA, Helbig JH, Zähringer U. 1996. Structure of a decasaccharide isolated by mild acid degradation and dephosphorylation of the lipopolysaccharide of *Pseudomonas fluorescens* strain ATCC 49271. *Carbohydr Res*. 283:129–139.

Knirel YA, Rietschel ET, Marre R, Zähringer U. 1994. The structure of the O-specific chain of *Legionella pneumophila* serogroup 1 lipopolysaccharide. *Eur J Biochem*. 221:239–245.

Knirel YA, Shashkov AS, Tsvetkov YE, Jansson PE, Zähringer U. 2003. 5,7-diamino-3,5,7,9-tetradeoxynon-2-ulosonic acids in bacterial glycopolymers: Chemistry and biochemistry. *Adv Carbohydr Chem Biochem*. 58:371–417.

Knirel YA, Vinogradov EV, L'Vov V L, Kocharova NA, Shashkov AS, Dmitriev BA, Kochetkov NK. 1984. Sialic acids of a new type from the lipopolysaccharides of *Pseudomonas aeruginosa* and *Shigella boydii*. *Carbohydr Res*. 133:C5–C8.

Lee SW, Sabet M, Um HS, Yang J, Kim HC, Zhu W. 2006. Identification and characterization of the genes encoding a unique surface (S-) layer of *Tannerella forsythia*. *Gene*. 371:102–111.

Leishman SJ, Do HL, Ford PJ. 2010. Cardiovascular disease and the role of oral bacteria. *J Oral Microbiol*. 21:2.

Lewis AL, Desa N, Hansen EE, Knirel YA, Gordon JI, Gagneux P, Nizet V, Varki A. 2009. Innovations in host and microbial sialic acid biosynthesis revealed by phylogenomic prediction of nonulosonic acid structure. *Proc Natl Acad Sci U S A*. 106:13552–13557.

Li X, Perepelov AV, Wang Q, Senchenkova SN, Liu B, Shevelev SD, Guo X, Shashkov AS, Chen W, Wang L, et al. 2010. Structural and genetic characterization of the O-antigen of *Escherichia coli* O161 containing a derivative of a higher acidic diamino sugar, legionaminic acid. *Carbohydr Res*. 345:1581–1587.

Logan SM, Hui JP, Vinogradov E, Aubry AJ, Melanson JE, Kelly JF, Nothaft H, Soo EC. 2009. Identification of novel carbohydrate modifications on *Campylobacter jejuni* 11168 flagellin using metabolomics-based approaches. *FEBS J*. 276:1014–1023.

Lowry RC, Parker JL, Kumbhar R, Mesnage S, Shaw JG, Stafford GP. 2014. The *Aeromonas caviae* AHA0618 gene modulates cell length and influences swimming and swarming motility. *Microbiologyopen*. doi:1002/mbo3.233.

MacLean LL, Vinogradov E, Pagotto F, Perry MB. 2011. Characterization of the lipopolysaccharide O-antigen of *Cronobacter turicensis* HPB3287 as a polysaccharide containing a 5,7-diacetamido-3,5,7,9-tetradeoxy-D-glycero-D-galacto-non-2-ulosonic acid (legionaminic acid) residue. *Carbohydr Res*. 346:2589–2594.

McNally DJ, Aubry AJ, Hui JP, Khieu NH, Whitfield D, Ewing CP, Guerry P, Brisson JR, Logan SM, Soo EC. 2007. Targeted metabolomics analysis of *Campylobacter coli* VC167 reveals legionaminic acid derivatives as novel flagellar glycans. *J Biol Chem*. 282:14463–14475.

McNally DJ, Schoenhofen IC, Houliston RS, Khieu NH, Whitfield DM, Logan SM, Jarrell HC, Brisson JR. 2008. CMP-pseudaminic acid is a natural potent inhibitor of PseB, the first enzyme of the pseudaminic acid pathway in *Campylobacter jejuni* and *Helicobacter pylori*. *ChemMedChem*. 3:55–59.

Megson ZA, Koerdt A, Schuster H, Ludwig R, Janesch B, Frey A, Naylor K, Wilson IB, Stafford GP, Messner P, et al. 2015. Characterization of an α-L-fucosidase from the periodontal pathogen *Tannerella forsythia*. *Virulence*. 6:282–292.

Morrison MJ, Imperiali B. 2014. The renaissance of bacillosamine and its derivatives: Pathway characterization and implications in pathogenicity. *Biochemistry*. 53:624–638.

Myneni SR, Settem RP, Connell TD, Keegan AD, Gaffen SL, Sharma A. 2011. TLR2 signaling and Th2 responses drive *Tannerella forsythia*-induced periodontal bone loss. *J Immunol*. 187:501–509.

Olivier NB, Chen MM, Behr JR, Imperiali B. 2006. In vitro biosynthesis of UDP-N,N'-diacetylbacillosamine by enzymes of the *Campylobacter jejuni* general protein glycosylation system. *Biochemistry*. 45:13659–13669.

Posch G, Pabst M, Brecker L, Altmann F, Messner P, Schäffer C. 2011. Characterization and scope of S-layer protein O-glycosylation in *Tannerella forsythia*. *J Biol Chem*. 286:38714–38724.

Rangarajan ES, Proteau A, Cui Q, Logan SM, Potetinova Z, Whitfield D, Purisima EO, Cygler M, Matte A, Sulea T, et al. 2009. Structural and functional analysis of *Campylobacter jejuni* PseG: A UDP-sugar hydrolase from the pseudaminic acid biosynthetic pathway. *J Biol Chem*. 284: 20989–21000.

Roy S, Honma K, Douglas CW, Sharma A, Stafford GP. 2011. Role of sialidase in glycoprotein utilization by *Tannerella forsythia*. *Microbiology*. 157:31953–31202.

Roy S, Phansopa C, Stafford P, Honma K, Douglas CW, Sharma A, Stafford GP. 2012. Beta-hexosaminidase activity of the oral pathogen *Tannerella forsythia* influences biofilm formation on glycoprotein substrates. *FEMS Immunol Med Microbiol*. 65:116–120.

Sakakibara J, Nagano K, Murakami Y, Higuchi N, Nakamura H, Shimozato K, Yoshimura F. 2007. Loss of adherence ability to human gingival epithelial cells in S-layer protein-deficient mutants of *Tannerella forsythensis*. *Microbiology*. 153:866–876.

Sára M, Sleytr UB. 2000. S-layer proteins. *J Bacteriol*. 182:859–868.

Schäffer C, Messner P. 2004. Surface-layer glycoproteins: An example for the diversity of bacterial glycosylation with promising impacts on nanobiotechnology. *Glycobiology*. 14:31R–42R.

Schäffer C, Messner P. Emerging facets of prokaryotic glycosylation. *FEMS Microbiol Rev*. doi:10.1033/femsre/fuw036.

Schirm M, Soo EC, Aubry AJ, Austin J, Thibault P, Logan SM. 2003. Structural, genetic and functional characterization of the flagellin glycosylation process in *Helicobacter pylori*. *Mol Microbiol*. 48:1579–1592.

Schoenhofen IC, Lunin VV, Julien JP, Li Y, Ajamian E, Matte A, Cygler M, Brisson JR, Aubry A, Logan SM, et al. 2006a. Structural and functional characterization of PseC, an aminotransferase involved in the biosynthesis of pseudaminic acid, an essential flagellar modification in *Helicobacter pylori*. *J Biol Chem*. 281:8907–8916.

Schoenhofen IC, McNally DJ, Brisson JR, Logan SM. 2006b. Elucidation of the CMP-pseudaminic acid pathway in *Helicobacter pylori*: Synthesis from UDP-N-acetylglucosamine by a single enzymatic reaction. *Glycobiology*. 16:8C–14C.

Schoenhofen IC, McNally DJ, Vinogradov E, Whitfield D, Young NM, Dick S, Wakarchuk WW, Brisson JR, Logan SM. 2006c. Functional characterization of dehydratase/aminotransferase pairs from *Helicobacter* and *Campylobacter*: Enzymes distinguishing the pseudaminic acid and bacillosamine biosynthetic pathways. *J Biol Chem*. 281:723–732.

Schoenhofen IC, Vinogradov E, Whitfield DM, Brisson JR, Logan SM. 2009. The CMP-legionaminic acid pathway in *Campylobacter*: Biosynthesis involving novel GDP-linked precursors. *Glycobiology*. 19:715–725.

Scott NE, Kinsella RL, Edwards AV, Larsen MR, Dutta S, Saba J, Foster LJ, Feldman MF. 2014. Diversity within the O-linked protein glycosylation systems of acinetobacter species. *Mol Cell Proteomics*. 13:2354–2370.

Sekot G, Posch G, Messner P, Matejka M, Rausch-Fan X, Andrukhov O, Schäffer C. 2011. Potential of the *Tannerella forsythia* S-layer to delay the immune response. *J Dent Res*. 90:109–114.

Sekot G, Posch G, Oh YJ, Zayni S, Mayer HF, Pum D, Messner P, Hinterdorfer P, Schäffer C. 2012. Analysis of the cell surface layer ultrastructure of the oral pathogen *Tannerella forsythia*. *Arch Microbiol*. 194:525–539.

Sekot G, Schuster D, Messner P, Pum D, Peterlik H, Schäffer C. 2013. Small-angle X-ray scattering for imaging of surface layers on intact bacteria in the native environment. *J Bacteriol*. 195:2408–2414.

Settem RP, Honma K, Nakajima T, Phansopa C, Roy S, Stafford GP, Sharma A. 2013. A bacterial glycan core linked to surface (S)-layer proteins modulates host immunity through Th17 suppression. *Mucosal Immunol*. 6:415–426.

Settem RP, Honma K, Sharma A. 2014. Neutrophil mobilization by surface-glycan altered Th17-skewing bacteria mitigates periodontal pathogen persistence and associated alveolar bone loss. *PLoS One*. 9:e108030.

Sharma A. 2010. Virulence mechanisms of *Tannerella forsythia*. *Periodontol 2000*. 54:106–116.

Socransky SS, Haffajee AD, Cugini MA, Smith C, Kent RL Jr. 1998. Microbial complexes in subgingival plaque. *J Clin Periodontol*. 25: 134–144.

Stafford GP, Chaudhuri RR, Haraszthy V, Friedrich V, Schäffer C, Ruscitto A, Honma K, Sharma A. in preparation. Draft genome sequences of three clinical isolates of *Tannerella forsythia* isolated from sub-gingival plaque from periodontitis patients in the USA. *Genome Announc*. 4:pii: e01286–16.

Stephenson HN, Mills DC, Jones H, Milioris E, Copland A, Dorrell N, Wren BW, Crocker PR, Escors D, Bajaj-Elliott M. 2014. Pseudaminic acid on *Campylobacter jejuni* flagella modulates dendritic cell IL-10 expression via Siglec-10 receptor: A novel flagellin-host interaction. *J Infect Dis*. 210: 1487–1498.

Tanner ACR, Listgarten MA, Ebersole JL, Strezempko MN. 1986. *Bacteroides forsythus* sp. nov., a slow-growing, fusiform *Bacteroides* sp. from the human oral cavity. *Int J Syst Bacteriol*. 36:213–221.

Thibault P, Logan SM, Kelly JF, Brisson JR, Ewing CP, Trust TJ, Guerry P. 2001. Identification of the carbohydrate moieties and glycosylation motifs in *Campylobacter* jejuni flagellin. *J Biol Chem*. 276: 34862–34870.

Tomek MB, Neumann L, Nimeth I, Koerdt A, Andesner P, Messner P, Mach L, Potempa JS, Schäffer C. 2014. The S-layer proteins of *Tannerella forsythia* are secreted via a type IX secretion system that is decoupled from protein O-glycosylation. *Mol Oral Microbiol*. 29:307–320.

Traving C, Schauer R. 1998. Structure, function and metabolism of sialic acids. *Cell Mol Life Sci*. 54:1330–1349.

Twine SM, Paul CJ, Vinogradov E, McNally DJ, Brisson JR, Mullen JA, McMullin DR, Jarrell HC, Austin JW, Kelly JF, et al. 2008. Flagellar glycosylation in *Clostridium botulinum*. *FEBS J*. 275:4428–4444.

Varki A. 1992. Diversity in the sialic acids. *Glycobiology*. 2:25–40.

Varki A, Cummings RD, Esko JD, Hudson FH, Stanley P, Bertozzi CR, Hart GW, Etzler ME. 2009. *Essentials of glycobiology*, 2nd ed. Cold Spring Harbor (NY), Cold Spring Harbor Laboratory Press.

Vinogradov E, Wilde C, Anderson EM, Nakhamchik A, Lam JS, Rowe-Magnus DA. 2009. Structure of the lipopolysaccharide core of *Vibrio vulnificus* type strain 27562. *Carbohydr Res*. 344:484–490.

Vinogradov EV, Shashkov AS, Knirel YA, Kochetkov NK, Dabrowski J, Grosskurth H, Stanislavsky ES, Kholodkova EV. 1992. The structure of the O-specific polysaccharide chain of the lipopolysaccharide of *Salmonella arizonae* O61. *Carbohydr Res*. 231:1–11.

Wilhelms M, Fulton KM, Twine SM, Tomas JM, Merino S. 2012. Differential glycosylation of polar and lateral flagellins in *Aeromonas hydrophila* AH-3. *J Biol Chem*. 287:27851–27862.

Zarschler K, Janesch B, Zayni S, Schäffer C, Messner P. 2009. Construction of a gene knockout system for application in *Paenibacillus alvei* CCM 2051^{T}, exemplified by the S-layer glycan biosynthesis initiation enzyme WsfP. *Appl Environ Microbiol*. 75:3077–3085.

Zunk M, Kiefel MJ. 2014. The occurrence and biological significance of the alpha-keto-sugars pseudaminic acid and legionaminic acid within pathogenic bacteria. *RSC Adv*. 4:3413–3421.